Abstract book

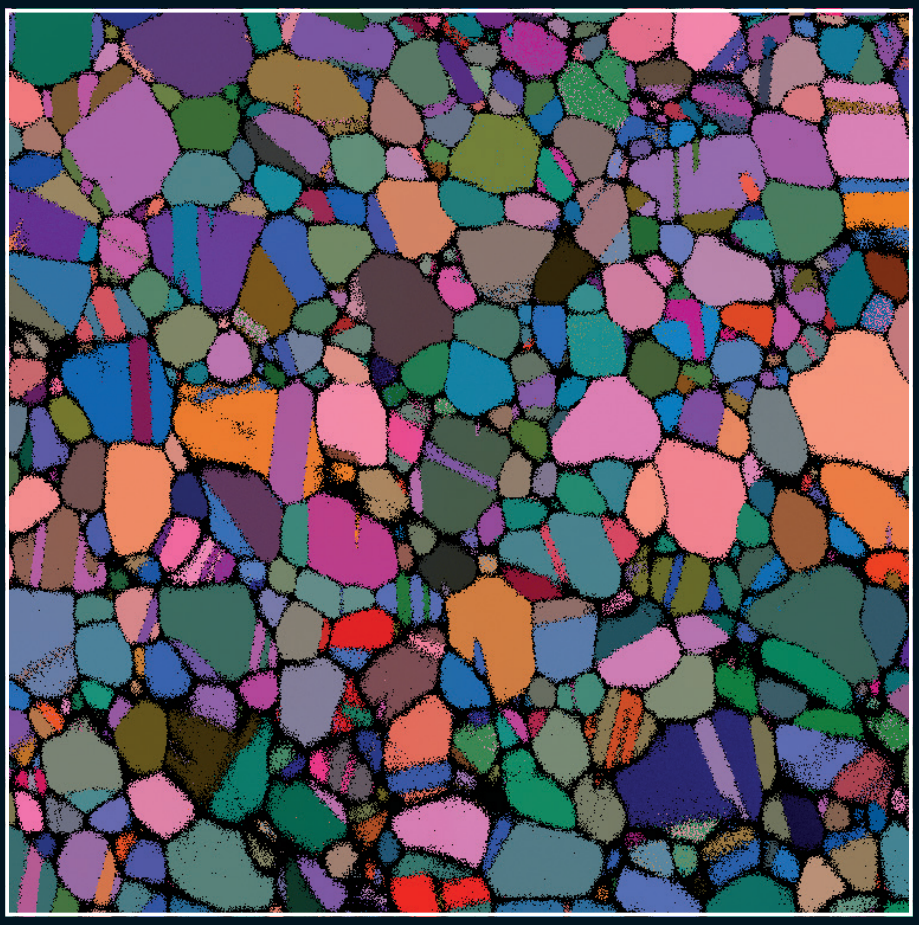

EMAG 2016

Electron Microscopy and Analysis Group Conference 2016

6–8 April 2016
Durham University, Durham, UK

Organised by the IOP Electron Microscopy and Analysis Group

http://emag2016.iopconfs.org

IOP Institute of Physics

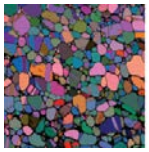

EMAG 2016

Electron Microscopy and Analysis Group Conference 2016

Programme

Wednesday 6 April

16:30	Welcome registration and exhibition *Earth Science Room*
18:30	(**Plenary) Analytical scanning transmission electron microscopy at atomic resolution** Professor Ferdinand Hofer, Graz University of Technology, Austria *Ken Wade Lecture Theatre*
19:30	*Close*

Thursday 7 April

08:00	Arrival refreshments *Earth Science Room*
08:30	**(Plenary) Electron tomography and multi-dimensional electron microscopy – progress and opportunities** Professor Paul Midgley, University of Cambridge, UK *Ken Wade Lecture Theatre*
09:30	Refreshments *Earth Science Room*

Session: Imaging and Diffraction I

10:00	**(Invited) Quantitative STEM - From composition to atomic fields** Andreas Rosenauer, Universität Bremen, Germany
10:30	**Extreme nanowires: The smallest crystals in the smallest nanotubes** Jeremy Sloan, University of Warwick, UK
10:45	**Realising fast two-dimensional pixelated STEM detectors** Magnus Nord, University of Glasgow, UK
11:00	**Probing atomic vibrations in graphene** Christopher Allen, University of Oxford, UK
11:15	**A twist on phase contrast in TEM** Laura Clark, EMAT, Universiteit Antwerpen, Belgium
11:30	**Flash presentations**
12:00	Lunch, poster session and exhibition *Earth Science Room*

Session: Applications I

14:00	**Electron irradiation of specimens heated in situ** Helen Freeman, University of Leeds, UK
14:15	**STEM cathodoluminescence mapping of surface traps in ZnO nanowires** Edward White, Imperial College London, UK
14:30	**High-resolution quantitative cathodoluminescence (CL) for material science and nanophotonics** David Gachet, Attolight AG, Switzerland
14:45	**Flash presentations**
15:30	Refreshments *Earth Science Room*

Session: Spectroscopy

16:00	**(Invited) Atomic configuration of hetoroatomic and functionalized carbon nanotubes probed via spatially-resolved EELS** Raul Arenal, Universite de Zaragoza, Spain
16:30	**Grain boundary segregation of P in Ni-base alloy** Jinsen Tian, University of Birmingham, UK
16:45	**ALCHEMI studies on Cr, Fe and Ni substitution in manganese cobaltite spinels** Mark Aindow, University of Connecticut, USA
17:00	**Is the electronic structure of few layer transition metal dichalcogenides two dimensional?** Jun Yuan, University of York, UK
17:15	**Flash presentations**
17:30	*Close and option of drinks in Earth Science Building.*
18:40	*Coach will depart Collingwood College to Castle*
19:00	*Reception and Conference Dinner*
22:00	*Coach returns delegates to Collingwood College*

Friday 8 April

08:30 Arrival refreshments
Earth Science Room

Session: Imaging and Diffraction II

09:00 **(Invited) Looking for the potential in digital large-angle electron diffraction patterns**
Richard Beanland, University of Warwick, UK

09:30 **Quantitative comparison of phase contrast imaging in conventional TEM focal series and STEM ptychography**
Emanuela Liberti, University of Oxford, UK

09:45 **Mapping the crystal morphology of graphene oxide with scanning electron diffraction**
Rowan Leary, University of Cambridge, UK

10:00 **STEM strain measurement from a stream of diffraction patterns recorded on a pixel-free delay-line detector**
Christoph Mahr, Universität Bremen, Germany

10:15 **Correlation of improved bioactivity of spray-pyrolysed glasses with structure from an electron diffraction study**
Yu-Jen Chou, University of Oxford, UK

10:30 Refreshments

Session: Applications II

11:00 **(Invited) Aberrated electron probes for magnetic spectroscopy with atomic resolution**
Jan Rusz, Uppsala University, Sweden

11:30 **In-situ formation study and oxidation of Fe nanoparticles in an aberration corrected E-(S)TEM**
Leonardo Lari, University of York, UK

11:45 **3D Ion beam tomography of nickel-base superalloys for morphological and spatial analysis**
Stephen Croxall, University of Cambridge, UK

12:00 Lunch, posters and exhibition

Session: Applications II (continued)

14:00	**Revealing local polarisation and domain configurations in ultrathin ferroelectric tunnel junctions by annular bright field STEM** Jonathan Peters, University of Warwick, UK
14:15	**Advances towards 2D and 3D quantitative STEM-EDX** Thomas Slater, University of Manchester, UK
14:30	**(Plenary) Advances in EELS for materials research** Alan Craven, University of Glasgow, UK
15:30	**Student awards**
15:50	Close

Flash presentations session - 11:30 – 12:00

FP:01 Recent developments in ptychography using a fast pixelated detector in the scanning transmission electron microscope
Gerardo T Martinez, University of Oxford, UK

FP:02 Effects of instrument imperfections on quantitative scanning transission electron microscopy
Marco Schowalter, University of Bremen, Germany

FP:03 The effect of oxygen on the contrast of ADF-STEM images
Ali Mostaed, University of Warwick, UK

FP:04 Time-resolved imaging and analysis of single atom diffusion on graphene oxide
Thomas Furnival, University of Cambridge, UK

FP:05 Angle-resolved scanning transmission electron microscopy employing an iris aperture
Andreas Rosenauer, Universität Bremen, Germany, Germany

Flash presentations - 14:45 – 15:30

FP:06 Quantitative analysis of damage mechanisms in pharmaceutical materials by transmission electron microscopy
James Cattle, University of Leeds, UK

FP:07 Ultrafast nano-fabrication and analysis using Xe plasma ion FIB-SEM microscope
Abdelmalek Benkouider, Tescan, Czech Republic

FP:08 Dispersed graphite and graphene nanoflakes in mesoporous carbon
Leonardo Lari, University of York, UK

FP:09 Structural and spectroscopic analysis of Mn doped Bi2Te3
Arsham Ghasemi, University of York, UK

FP:10 Size distribution investigations of thiol-stabilised silver nanoparticles
Julie Watts, University of Nottingham, UK

FP:11 Direct observation of in-situ sublimation of tellurium nanowires
Sam Marks, University of Warwick, UK

FP:12 Optimising automated quantification of nanoparticle compositions using scanning transmission electron microscope spectrum imaging
Yichi Wang, University of Manchester, UK

FP:13 Simulated HAADF-STEM + EDS Tomography of Sub-22 nm FinFETS
Richard Aveyard, TU Delft, The Netherlands

FP:14 Quantitative structural and compositional studies of catalyst nanoparticles using annular dark field imaging and spectroscopy
Aakash Varambhia, University of Oxford, UK

Flash presentations – 17:15 – 17:30

FP:15 Modal Decomposition for 2D and 3D STEM-EELS Analyses of surface plasmons in gold and silver nanoparticles
Sean Collins, University of Cambridge, UK

FP:16 Systematic study of background subtraction techniques for EELS
Veerendra C Angadi, The University of Sheffield, UK

FP:17: The effect of prior deformation on the phase evolution and phosphorus segregation within an AISI Type 316 austenitic stainless steels,
Ana Martinez-Ubeda, University of Bristol Interface Analysis Centre, UK

Posters

P:01 Recent developments in ptychography using a fast pixelated detector in the scanning transmission electron microscope
Gerardo T Martinez, University of Oxford, UK

P:02 Effects of instrument imperfections on quantitative scanning transission electron microscopy
Marco Schowalter, Universität Bremen, Germany

P:03 The effect of oxygen on the contrast of ADF-STEM images
Ali Mostaed, University of Warwick, UK

P:04 Time-resolved imaging and analysis of single atom diffusion on graphene oxide
Thomas Furnival, University of Cambridge, UK

P:05 Angle-resolved scanning transmission electron microscopy employing an iris aperture
Knut Müller-Caspary, Universität Bremen, Germany

P:06 Quantitative analysis of damage mechanisms in pharmaceutical materials by transmission electron microscopy
James Cattle, University of Leeds, UK

P:07 Ultrafast nano-fabrication and analysis using Xe plasma ion FIB-SEM microscope
Abdelmalek Benkouider, Tescan, Czech Republic

P:08 Dispersed graphite and graphene nanoflakes in mesoporous carbon
Leonardo Lari, University of York, UK

P:09 Structural and spectroscopic analysis of Mn doped Bi2Te3
Arsham Ghasemi, University of York, UK

P:10 Size distribution investigations of thiol-stabilised silver nanoparticles
Julie Watts, University of Nottingham, UK

P:11 Direct observation of in-situ sublimation of tellurium nanowires
Sam Marks, University of Warwick, UK

P:12 Optimising automated quantification of nanoparticle compositions using scanning transmission electron microscope spectrum imaging
Yichi Wang, University of Manchester, UK

P:13 Simulated HAADF-STEM + EDS Tomography of Sub-22 nm FinFETS
Richard Aveyard, TU Delft, The Netherlands

P:14 Quantitative structural and compositional studies of catalyst nanoparticles using annular dark field imaging and spectroscopy
Aakash Varambhia, University of Oxford, UK

P:15 Modal Decomposition for 2D and 3D STEM-EELS analyses of surface plasmons in gold and silver nanoparticles
Sean Collins, University of Cambridge, UK

P:16 Systematic study of background subtraction techniques for EELS
Veerendra C Angadi, The University of Sheffield, UK

P:17 STEM cathodoluminescence mapping of surface traps in ZnO nanowires
Edward White, Imperial College London, UK

P:18 How does the carbon source affect carbon nanotube chirality in floating catalyst CVD?
Jonathan Barnard, University of Cambridge, UK

P:19 Electron nanofocusing using perforated nanoparticles
Guenter Möebus, University of Sheffield, UK

P:20 Electron beam writing in oxide glasses via irradiation induced metal nanodots
Guenter Möebus, University of Sheffield, UK

P:21 Dynamical and thermal properties of the rocksalt MgS and MgSe compounds
Yassine Chaouche, Université Larbi Tebessi, Algeria

P:22 Elongated silicon–carbon bonds at graphene edge
Qu Chen, University of Oxford, UK

P:23 Understanding the epitaxial growth mechanisms of metal oxide nanoislands on strontium titanate substrates via transmission electron microscopy
Xuan Cheng, University of New South Wales, Australia

P:24 Determining optimum sample thickness for TKD using AZtec
Keith Dicks, Oxford Instruments, UK

P:25 Chemical and structure analysis of soft and bio-materials
Meiken Falke, Bruker, Germany

P:26 Thermally induced dynamics of dislocations in graphene at atomic resolution
Chuncheng Gong, University of Oxford, UK

P:27 Aberration corrected electron energy loss spectroscopy analysis of irradiated UO_2 epitaxial film
Ian Griffiths, University of Bristol, UK

P:28 On the HREM contrast from 0001 planes in wurtzite GaAs
Crispin Hetherington, Lund University, Sweden

P:29 Accurate EPMA quantification of the first series transition metals using lines
Ian Holbort, Acutance Scientific Ltd, UK

P:30 Evaluating the electron beam sensitivity of calcium carbonate based materials
Robert Hooley, University of Leeds, UK

P:31 Structure study of mesoporous silica templates by phase restoration of focal series of images
Reza J Kashtiban, University of Warwick, UK

P:32 Insight into the physical chemistry of nanoalloys from aberration-corrected HAADF-STEM
Ziyou Li, Nanoscale Physics Research Laboratory, UK

P:33 Atomic structure of 1.8 nm monolayer-protected AuN clusters by aberration-corrected STEM
Jian Liu, University of Birmingham, UK

P:34 Generation of clusters in reflection mode from the Matrix Assembly Cluster Source (MACS)
Jian Liu, University of Birmingham, UK

P:35 Pt diffusion dynamics on the formation Cr-Pt Core-Shell nanoparticles
Jian Liu, University of Birmingham, UK

P:36 Transition radiation artefacts in TEM-CL imaging and spectroscopy
Budhika Mendis, University of Durham, UK

P:37 Correlation between the atomic structure and spin-polarization at Co_2MnSi/Ag epitaxial interfaces
Zlatko Nedelkoski, University of York, UK

P:38 Oxides in austenitic alloys exposed to PWR primary water: mapping oxidation states with EELS
Gemma Pimentel, University of Oxford, UK

P:39 Characterisation of hydrogen stabilised polar MgO(111) thin films on 6H-SiC(0001)
Daniel Pingstone, University of York, UK

P:40 HRTEM study of agglomeration of ZnO nanoparticles by oriented attachment
David Rickerby, European Commission Joint Research Centre, Italy

P:41 3D structure mapping using a two-dimensional pixelated STEM detector
Andrew Ross, University of Glasgow, UK

P:42 Aberration measurement in a probe-forming system using graphene
Hidetaka Sawada, University of Oxford, UK

P:43 Off-axial aberration measurement for the image-forming system of a hexapole type aberration corrector
Hidetaka Sawada, University of Oxford, UK

P:44 Planar FIB milling of copper by using the novel rocking stage technology
Sharang Sharang, Tescan Orsay Holding, Czech Republic

P:45 Wear behaviour of high-performance C-Mo-W coatings investigated by multi-technique aberration corrected TEM
Joanne Sharp, University of Sheffield, UK

P:46 Quantitative grain boundary analysis with atom probe tomography and t-EBSD (TKD)
Robert Ulfig, CAMECA Instruments Inc., USA

P:47 Detailed atomic reconstruction of extended line defects in monolayer MoS_2
Shanshan Wang, University of Oxford, UK

P:48 Investigation of phase separation in InGaN semiconductor alloys by plasmon loss spectroscopy
Xiaoyi Wang, University of Sheffield, UK

Oral abstracts

Wednesday 6 April

(Plenary) Analytical scanning transmission electron microscopy at atomic resolution

F Hofer [1], W Grogger[1], G Haberfehlner[2], F Schmidt[1], D Knez[1], M Albu[2], A Orthacker[2], C Gspan[2] and G Kothleitner[1]

[1]Graz University of Technology, Austria, [2]Graz Centre for Electron Microscopy, Austria

Scanning transmission electron microscopy (STEM) has proven to be an indispensable method for mapping the location and identity of atoms in complex materials. The introduction of spherical aberration correction paved the way for atomic resolution imaging on a routine basis using high-angular annular dark field (HAADF) and annular bright field (ABF) detectors.

The aberration corrected STEM also enables atomic-resolution mapping of the individual elements in a material (elemental mapping) thus allowing a correlation of structural and chemical information by means of electron energy-loss spectrometry (EELS) and energy dispersive X-ray spectrometry (EDX).

However, quantification of atomic resolution elemental maps on an absolute scale remains a challenge. In most cases elemental maps at atomic resolution could only be interpreted qualitatively. Using a novel simultaneous EELS and EDX spectrum image acquisition approach, it is now possible to explore elemental quantification in terms of volumetric densities [1]. Absolute scale quantification comparisons between experiment and quantum mechanical calculations show that it is possible to determine the number of atoms in the individual atom columns, but only if all scattering effects are fully considered [2]. The progress in elemental mapping at atomic resolution will be highlighted and practical consequences for solving materials problems will be discussed [3].

Additionally, we will show how electron tomography can be used for 3D elemental mapping using simultaneous EELS and EDX spectroscopy at the nanometre scale [4]. Advancing electron tomography to atomic resolution reveals the 3D morphology and composition of Ag/Au core/shell nanoparticles grown in superfluid helium nanodroplets. Atomic positions could be estimated without using any prior information and with minimal filtering [5].

Finally, we will report on new STEM-EELS experiments of the plasmonic properties of a silver thin film taper, demonstrating that the focused plasmon field at the taper tip is fueled by edge modes [6]. Electron tomography in combination with STEM-EELS experiments and simulations was used to unravel the interplay between structure and plasmonic properties of a silver nano-cuboid dimer [7].

This research has received funding from the European Union within the 7th Framework Programme [FP7/2007-2013] under Grant Agreement no. 312483 (ESTEEM2).

[1] G Kothleitner et al., *Microsc. Microanal.* 20 (2014) 678-686
[2] G Kothleitner et al., *Phys. Rev. Letters*, 112 (2014) 085501, 1-5
[3] Z Chen, Ultramicroscopy 157 (2015) 21-26
[4] G Haberfehlner et al., *Nanoscale* 6 (2014) 14563-9
[5] G Haberfehlner et al., *Nature Comm.* 6 (2015) 8779
[6] F P Schmidt et al., *Optics Letters* 40 (2015) 5670
[7] G Haberfehlner et al., *Nanoletters* 15 (2015) 7726-7730

Thursday 7 April

(Plenary) Electron tomography and multi-dimensional electron microscopy – progress and opportunities

P A Midgley

University of Cambridge, UK

In this presentation I will consider the progress made in electron tomography and related forms of 'multi-dimensional' electron microscopy (MDEM), especially as applied to materials and devices at the nanoscale. The rise in popularity of electron tomography in the physical sciences has come about through advances in microscope hardware, and the increased flexibility in controlling the beam and collecting scattered electrons, and the vast increase in computational power that has allowed for a more detailed and rapid analysis and reconstruction of large data sets. In addition, the introduction of fast, efficient x-ray and energy loss spectrometers has added a new dimension to tomographic analysis that has led to the possibility of mapping at the nanoscale not just morphology but also composition, chemistry, electronic properties and optical properties in three dimensions.

In order to optimise the analysis of such multi-dimensional 'big data' sets, novel software approaches and reconstruction codes have been developed. This allows, on the one hand, the possibility of enormous *data* reduction and an improved means to extract the salient 3D *information*, and on the other, offers an opportunity to change the way in which the data is collected in the first place, through more efficient mapping strategies and alternative dose-fractionation methodologies.

Throughout the presentation I will give recent examples of how electron tomography and MDEM has been applied across the materials science spectrum, with application to catalysis, superalloys, semiconductor nanostructures and plasmonics. By incorporating prior information into the reconstruction process, the fidelity of the tomograms is shown to be greatly improved and this leads naturally towards a model-based reconstruction methodology incorporating a more detailed description of beam-sample interactions than is possible in a simple back-projection approach. The presentation will end with a look to the future and how tomography and MDEM may develop further over the next few years.

Session: Imaging and Diffraction I

(Invited) Quantitative STEM - From composition to atomic fields

A Rosenauer[1], K Müller-Caspary[1], M Schowalter[1], T Grieb[1], F F Krautz[1], T Mehrtens[1], A Béché[2], J Verbeeck[2], J Zweck[3], S Löffler[4] and P Schattschneider[4]

[1]Universität Bremen, Germany, [2]University of Antwerp, Belgium, [3]Universität Regensburg, Germany, [4]Vienna University of Technology, Austria

The image intensity in HAADF STEM images shows a strong chemical sensitivity. As it is also influenced by specimen thickness, crystal orientation as well as characteristics of illumination and detector a standard-free quantification of composition requires a comparison with accurate image simulation, for which we use the frozen lattice approach of the STEMsim program. The experimental intensity of atom columns obtained by image segmentation is normalized with respect to the incident electron beam and compared with simulations, from which we are able to measure specimen thickness or composition. As examples of application we demonstrate measurement of segregation efficiency in InGaAs layers buried in GaAs and quantification of few atomic percent of nitrogen in GaNAs. We also show that a combination of measurement of strain and HAADF image intensity can be used to determine both In and N compositions in quaternary InGaNAs. Acquiring two STEM images of the same area with different angular ranges of the detector yields two sources of information which can be exploited, e.g. to evaluate specimen thickness

and composition independently. We will also very briefly point out the effect of instrumental imperfections on quantitative STEM results.

In the second part of the talk we present results on measurement of atomic electric fields. The applied technique does not rely on the assumption that the ronchigram has uniform intensity and is shifted as a whole by the action of the electric field, which is the base for differential phase contrast (DPC) technique (Nature Phys. 8, 611 (2012)). Our approach to quantify atomic electric fields is based on recording a ronchigram for each scan position on a pixelated CCD camera, combined with a simple but stringent quantum mechanical interpretation (Nat. comm. 5, 5653 (2014)). The intensity I(px,py) in a certain pixel of the recorded ronchigram is proportional to the probability that the corresponding momentum (px,py) is observed. Thus the center-of gravity-type summation $\langle p \rangle = \int I(px,py)$ dpxdpy yields the expectation value for the momentum. We show how the momentum transfer can be related to the projected electric field convolved with the intensity of the STEM probe in thin specimens.

Extreme nanowires: The smallest crystals in the smallest nanotubes

J Sloan[1], R J Kashtiban[1], S Marks[1], A M Sanchez[1], R Beanland[1], S Brown[1], A Vasylenko[1], D Quigley[1], P Brommer[1], K Morawiec[2], S Kret[2], P V C Medeiros[3], A J Morris[3], J H Spencer[4], DC Smith[4] and Q Ramasse[5]

[1]University of Warwick, UK, [2]Polish Academy of Sciences, Poland, [3]University of Cambridge, UK, [4]University of Southampton, UK, [5]SuperSTEM Laboratory, UK

A logical extension to fabrication of monolayer 2D materials such as graphene is creation of 'Extreme Nanowires' (i.e. Fig. 1(a)), down to a single atom column in width.[1,2] In this limit, crystals have fundamentally different physical characteristics and properties.[3-5] We and others have created a atomically regulated nanowires by confining them within the smallest diameter carbon nanotubes (i.e. either single walled carbon nanotubes (SWNTs) or double walled carbon nanotubes (DWNTs)), and are investigating their structural and electronic properties. These materials also provide an ultimate benchmark for testing the most sensitive characterisation methodologies which, when corroborated with suitable theory, will provide new data on physics at the most fundamental length scale accessible to nanomaterials fabrication. The most powerful investigative tools for structural investigation are aberraton-corrected Transmission Electron Microscopy (ac-TEM) and Scanning Transmission Electron Microscopy (ac-STEM) and, here, we describe the application of these methods to a variety of Extreme Nanowire systems.

One of the most crucial aspects of the role of electron microscopy in our investigation is the 2D and 3D elucidation of the structure of quasi- or true 1D nanowires formed in SWNTs as these form the primary source of information for density functional theory (DFT) and other ab initio theoretical approaches to both structure and properties elucidation. When combined with real physical measurements, this combined approach becomes even more powerful as we can start to piece together how the fundamental physics of a crystalline nanowire changes once we constrain its width down to one or two atoms in cross section. For example we recently record Raman Spectra from 2x2 atom thick HgTe nanowires embedded within 1.2-1.4 nm SWNTs[4] and found that we are able to model the Raman-measured lattice phonons of this system based on a simple structural model previously determined from two pairs of Exit Wave Reconstruction images which we also used to make DFT predictions about the altered electronic structure of this system which is predicted to change from a -0.3 eV semi-metal to a ~1.2 eV band gap semiconductor.[3] Following on from the exciting recent work of Senga et al.[2] who imaged the first true 1D crystals of CsI in DWNTs we are now modeling single atomic chain coils of tellurium formed within narrow SWNTs.[6]

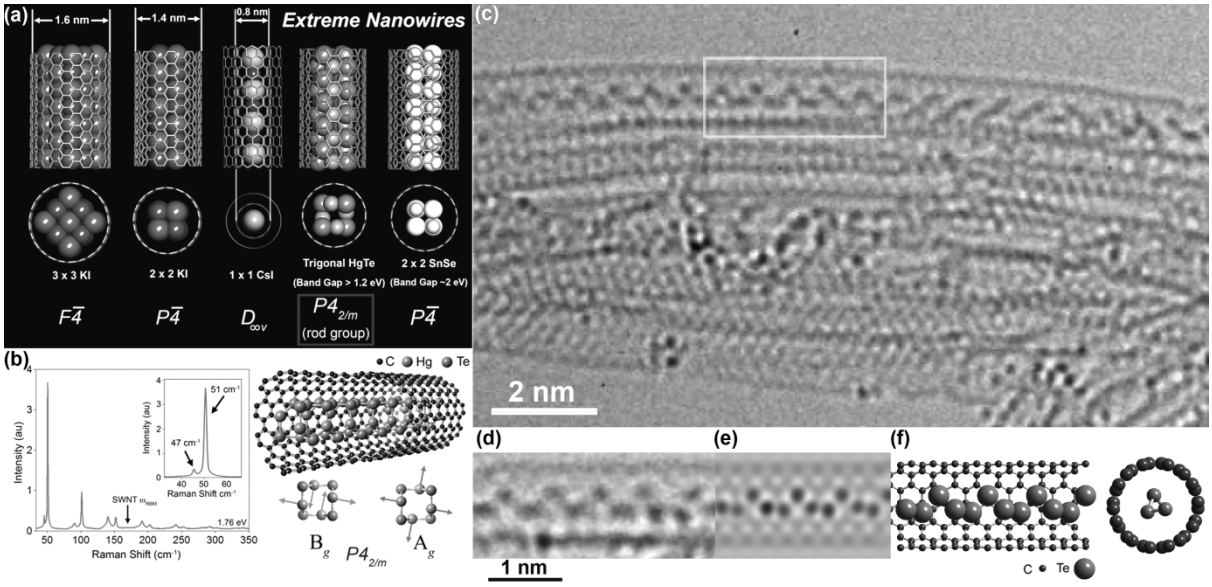

Figure 1. a) A selection of 'Extreme Nanowires' grown in Single Walled carbon Nano-Tubes (SWNTs) described by us and others, including 3x3 KI (rocksalt), 2x2 KI (rocksalt), 1x1 CsI, distorted 2x2 HgTe and 2x2 SnSe. These structures take on novel symmetries, as indicated below. b) Raman Spectrum of bundles of SWNTs filled with the distorted 2x2 HgTe structure at a laser energy of 1.76 eV. Inset at right is the composite HgTe@SWNT crystal structure previously solved by ac-TEM (actually exit wave reconstruction). Proposed B_g and A_g symmetry measured lattice phonons predicted by theory. (c) ac-TEM image of SWNTs partially filled with quasi-1D 'coils' of Te atoms, a single atomic coil per SWNT. (d) detail from (c). (e) Multislice image simulation based on a structural match produced by ab initio random structure searching (AIRSS). (e) AIRSS model for coiled Te atomic chain in a narrow SWNT.

[1] J Sloan *et al* Chem Commun (2002) 1319
[2] R Senga *et al* Nature Mater 13 (2014) 1050
[3] R Carter *et al* Phys Rev Lett 96 (2006) 21550
[4] J H Spencer *et al* ACS Nano 8 (2014) 9044
[5] C Giusca *et al* Nano Lett 13 (2013) 2040
[6] To be published

Realising fast two-dimensional pixelated STEM detectors

M Nord, G W Paterson, D McGrouther and I MacLaren

University of Glasgow, UK

Scanning Transmission Electron Microscopy (STEM) is a well-established technique for imaging and characterising materials at sub-Ångström spatial resolutions. The convergent beam electron diffraction pattern in the back focal plane contains a wealth of information. However, in most STEM imaging techniques, a large fraction of the scattered electrons is integrated into a single value for each scan position. While this enables very fast acquisition, it also discards much of the rich information in the back focal plane. Recently, the advent of fast direct electron counting systems has enabled the development of two-dimensional pixelated STEM detectors, which acquire large parts of the back focal plane at high frame rates. While this opens up many exciting possibilities, the field is far from mature and there remain many technical issues with how to use the large 4-D datasets optimally.

In this presentation, we focus on recent software and hardware developments for practically using a fast pixelated

detector capable of 1100 frames per second. It will cover how we have made it possible to get live or near-live images into Digital Micrograph through using standard and open network components and by offloading the data processing to a mix of graphical and central processing units. This enables a variety of images to be generated simultaneously through synthetic apertures and more advanced techniques. Examples will be given of how processing is handled for doing live bright field, annular dark field and differential phase-contrast imaging of magnetic materials. We will also touch on the file format chosen for data storage and ways of visualising this kind of 4-D data.

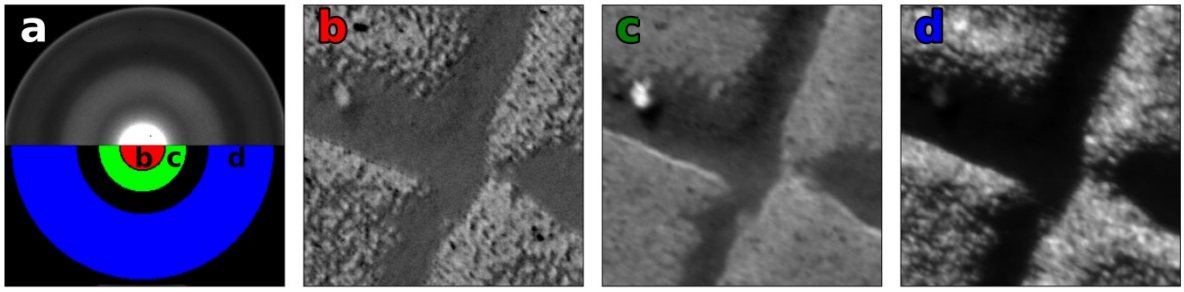

Application of synthetic apertures to a 4-D dataset acquired on a Au/C sample. (a) Sum of all the convergent beam electron diffraction images. Red, green and blue areas show the synthetic apertures used in (b), (c) and (d), which show the resulting STEM images.

Probing atomic vibrations in graphene

C S Allen, H Sawada and A I Kirkland

University of Oxford, UK

Using a technique based on the analysis of electron diffraction patterns, [1] we have recently measured both the in-plane and out-of-plane mean square displacement (MSD) of carbon atoms from their ideal lattice position in monolayer graphene.[2] Comparison of these experimental measurements with theoretical calculations have indicated significant and surprising limitations on the phonon wavelength in our mono-layer graphene samples.

We extend this work by considering the limitations of these measurements set by the precise optics of the microscope and any unintentional sample tilt. By tracking specific reflections in tilt series diffraction patterns we determine the shape of the graphene 'relrods'.[3] Comparison with simulation allow us to extract tilt-independent values for the in-plane MSD. We also investigate the effect of varying coherence, parallelicity and effective illumination area of the incident beam and comment on the possibility of using these techniques to probe local atomic vibrations in nanomaterials.

[1] B Shevitski et al. Phys. Rev. B. 87,045417, (2013)
[2] C S Allen et al. J. Appl. Phys, 118, 074302 (2015)
[3] P Kumar et al. Nat. Comm., 6, 1-7 (2015)

A twist on phase contrast in TEM

L Clark and J Verbeeck

Universiteit Antwerpen, Belgium

Images of beam-sensitive materials are generally limited to resolutions well below microscope abilities, due to the imposed low-dose imaging requirements and the accompanying low SNR..To overcome these SNR problems, image contrast must be increased. The two main prongs of attack to improve imaging of beam-sensitive phase objects, are either to manipulate the amplitude in the diffraction plane (such as with Schlieren imaging), or to manipulate the phase profile in the diffraction plane (such as with the so-called Volta phase plate [1]).

While huge advances have been made over the last decade in experimental phase plates, with a veritable zoo of feasible designs now produced [2], we investigate a phase plate not based on the usual Zernike model [3], but instead a spiralling phase structure may lead to improved contrast and edge detection in the imaging plane [4].

Here we systematically study the SNR behaviour of the various existing phase plate methods, and compare to the performance when imaging with a spiral phase plate. We find the spiral phase plate leads to significantly enhanced image contrast, which may enable imaging of the important features of an object above the noise floor, at a lower dose than is currently feasible.

Slight variations in the use of the spiral phase plate can enable different structures of contrast to display in the resultant image – we suggest uses for this novel contrast mechanism and how the spiral phase plate may be combined with existing low dose imaging methods to further increase image quality while avoiding beam damage.

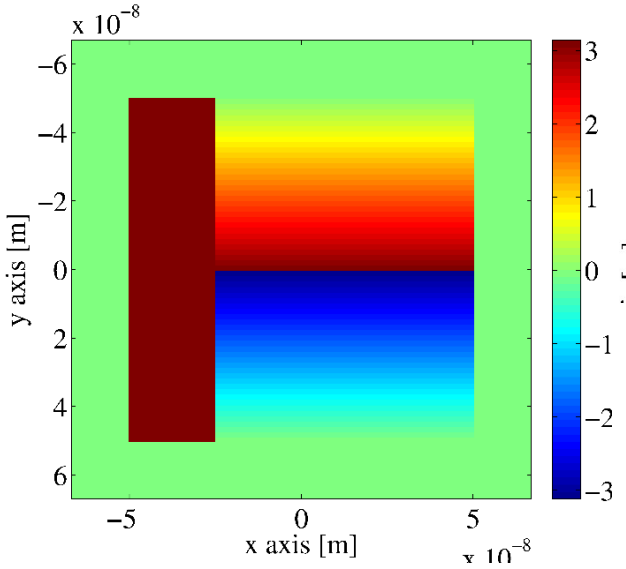

Figure 1: Weak Phase Object Sample

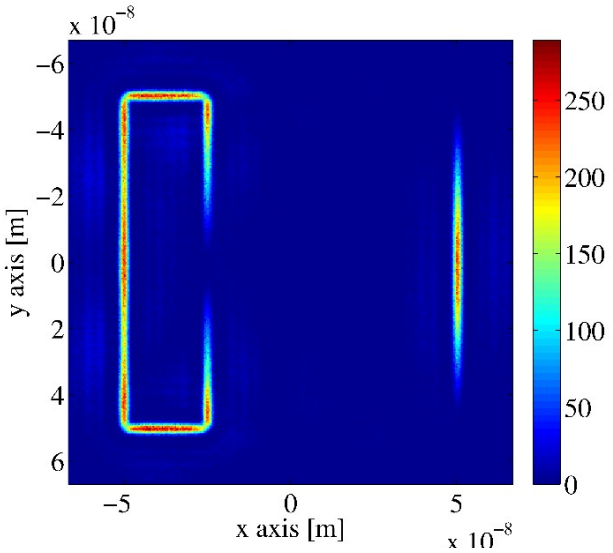

Figure 2: Resulting Image Contrast at low dose

[1] D Radostin, et al., PNAS, 111.44 (2014): 15635-15640.

[2] For a summary of the options see: Frindt, N., “Development and implementation of electrostatic Zach phase plates for phase contrast transmission electron microscopy”, Ph.D. thesis, U. Heidelberg, 2013.

[3] Born, Max, and Emil Wolf. "Principles of Optics, 7th (expanded) ed." (1999): 790-852.

[4] Blackburn, A. M., and J. C. Loudon. Ultramicroscopy 136 (2014): 127-143. L. C and J. V. acknowledge funding from the European Research Council under the 7th Framework Program (FP7), ERC Starting Grant No. 278510—VORTEX.

Session: Applications I

Electron irradiation of specimens heated in situ

H M Freeman, A J Scott and R M Drummond-Brydson

University of Leeds, UK

Graphite moderated nuclear reactors operate at temperatures around 350°C to reduce the degree of irradiation damage through continual thermal annealing. The temperature at which annealing occurs is dependent on the irradiation temperature. Understanding the damage processes experienced by irradiated nuclear graphite is essential in predicting the lifetime of the material, which influences the overall lifetime of the reactor. Here electron irradiation is used as a surrogate for neutron irradiation.

The effect of electron radiation of nuclear graphite within a transmission electron microscope at -190°C to 200°C has been investigated. For each temperature, 'Pile Grade A' graphite specimens were subject to ca. 10^{22} electrons cm^{-2}, and transmission electron micrographs and selected area diffraction patterns were collected during beam exposure. By considering a critical fluence, at which the d-spacing increased by 10%, a temperature threshold was determined (Figure 1). Below ca. 150°C, electron radiation significantly damaged the atomic structure, observed through fragmented basal planes, a tortuous nanotexture, and a >10% increase in d-spacing. Above ca. 150°C the effects of thermal annealing became more prevalent so that the nanostructure was maintained for much higher fluences. Data was compared to the work of Muto and Tanabe (1999[1].

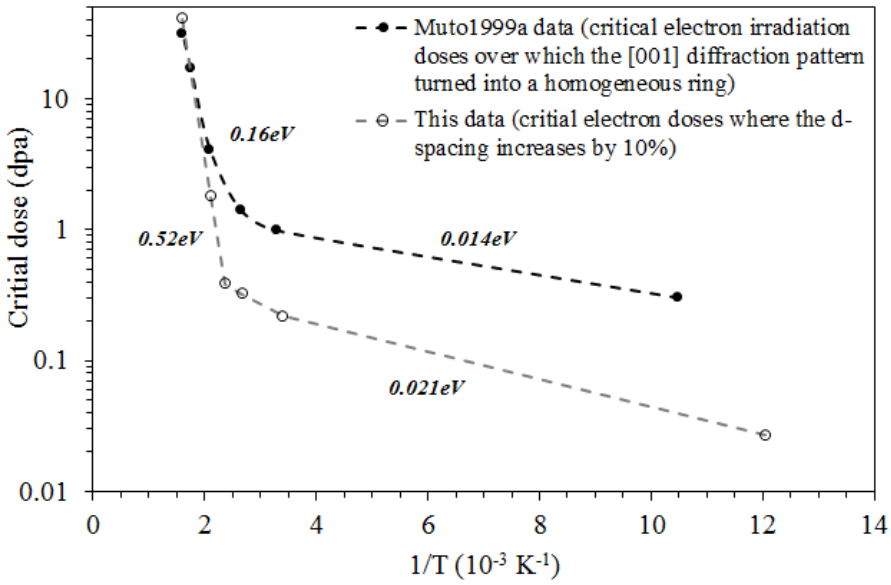

Figure 1 Arrhenius plot of the critical dose for different temperatures, with corresponding activation energies labelled. Data is plotted from this study and from that presented by Muto & Tanabe (1999) [1]. Data sets have been extrapolated to show the critical dose at 350°C (1.6×10^{-3} K^{-1}).

[1] M S, Tanabe T. Fragmentation of graphite crystals by electron irradiation at elevated temperatures. J Electron Microsc (Tokyo) 1999;48:519–23

STEM cathodoluminescence mapping of surface traps in ZnO nanowires

E R White[1], O W Kennedy[2], M Coke[2], P A Warburton[2] and M S P Shaffer[1]

[1]Imperial College London, UK, [2]University College London, UK

ZnO is an attractive material for electronic and optoelectronic applications due to its wide bandgap, large exciton binding energy, highly efficient emission, and chemical stability [1]. While a variety of different nanostructure morphologies have been reported, the large surface area-to-volume ratio means surface defects often deteriorate performance. Understanding the spatial distribution of surface traps and how to minimize their concentration is critical to engineering future nanoscale ZnO devices.

As shown in Figure 1, we use hyper-spectral STEM cathodoluminescence (CL) imaging to show that defect emission in high quality ZnO nanowires emanates from the surface. Figures 1b and 1c are constructed by integrating the CL intensity over the indicated energy range. A comparison of the resultant maps with the HAADF image (Figure 1a) reveals emission around 3.3 eV is strongest in the nanowire core, and emission between 2.0-3.0 eV is strongest on the edges of the nanowire. The 3.3 eV emission corresponds to the bandgap, and the broad emission between 2.0-3.0 eV is related to defects [1]. At the edges of the nanowire the electron beam-surface interaction is maximized; thus Figure 1c shows surface defects are responsible for the broad emission. Further analysis demonstrates that higher energy defect emission within the 2.0-3.0 eV range is more tightly confined to the surface.

Similar measurements on ZnO nanowires with ternary ZnMgO shells show no detectable emission below 3.0 eV. The lack of any defect emission indicates the ZnMgO shell passivates the surface, which represents a critical step towards improving conductivity in ZnO nanowires [2].

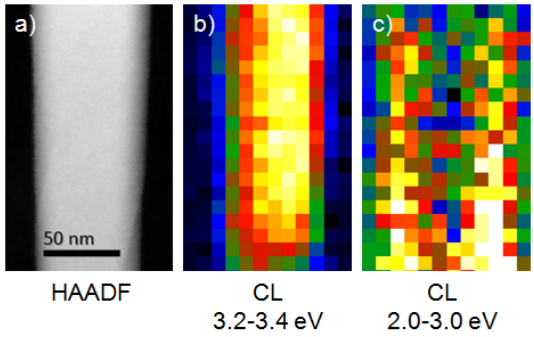

Figure 1: (a) HAADF image of a ZnO nanowire. (b) CL map of the 3.3 eV bandgap emission. (c) CL map of the 2.0-3.0 eV defect emission. Each pixel in a CL map contains a CL spectrum; (b) and (c) are generated by integrating the spectra over the indicated energies, and are normalized to each map's maximum intensity.

[1] Djurisić, A B and Leung, Y H Optical properties of ZnO nanostructures. *Small*. 3, 477-481 (2008)
[2] The authors acknowledge funding from EPSRC grant number EP/K035274/1, and the Experimental Techniques Centre at Brunel University for use of the STEM-CL system

High-resolution quantitative cathodoluminescence (CL) for material science and nanophotonics

D Gachet

Attolight AG, Switzerland

High spatial resolution spectroscopic information may be acquired by using an electron beam in a modern scanning electron microscope (SEM), exploiting a phenomenon called cathodoluminescence (CL). CL can be used to perform non-destructive analysis of a broad range of materials comprising insulators, semiconductors and metals. This approach offers several advantages over usual optical spectroscopy techniques. The multimode imaging capabilities of the SEM enable the correlation of optical properties (*via* CL) with surface morphology (secondary electron – SE – mode) at the nanometer scale [1]. In semiconductors and insulators, the CL spectrum gives local information on the electronic bandgap and defect states. In metals and nanostructured materials, CL is sensitive to the local density of optical states (LDOS) [2] and allows direct probing of nanophotonic devices.

We will show how high resolution hyperspectral CL microscopy is routinely used to perform defect and homogeneity metrology as well as failure analysis in semiconducting materials. Examples on optoelectronic [3,4] and solar cells devices [5] will be highlighted. In addition, we will give examples of CL imaging of nanophotonic structures used as single photon sources [6], or for lasing [7] and sensing applications [8]. Finally, we will show how the introduction of pulsed electron excitation and time resolved detection of the CL signal (TRCL) allows carrier dynamic probing at the nanoscale [9].

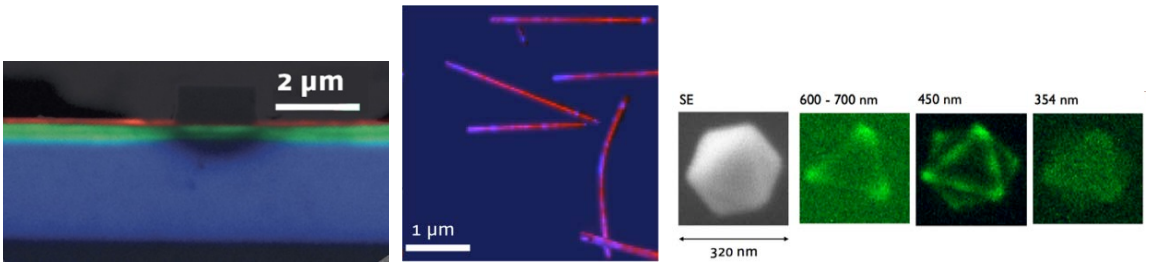

Figure 1. Application of CL (a) for failure analysis (aged InGaN/GaN green laser diode, adapted from Ref. [4]), (b) for imaging quantum dots in nanowires (courtesy of Prof. Fontcuberta, EPFL) and (c) for plasmon imaging in metal nanoparticles (adapted from Ref. [8]).

[1] L Reimer in “Scanning Electron Microscopy”, (Springer, Berlin) Ch. 1
[2] M Kociak and O. Stéphan, Chem. Soc. Rev 43 (2014), p. 3865
[3] Iwata et *al*, J. Appl. Phys. 117 (2015), p. 115702
[4] Mendis et *al*, Phys. Rev. Lett. 115 (2015), p. 218701
[5] De Santi et *al*, IEEE Trans. Nanotech. (in press)
[6] Fontana et *al*, Phys. Rev. B 90 (2014), p. 075307
[7] Puchtler et *al*, ACS Photonics 2 (2015), p. 137
[8] Liu et *al*, Small 10 (2014), p. 4940
[9] Shahmohammadi et *al*, Nano Lett. 16 (2016), p. 243

Session: Spectroscopy

(Invited) Atomic configuration of hetoroatomic and functionalized carbon nanotubes probed via spatially-resolved EELS

R Arenal

Universidad de Zaragoza, Spain

The modification of the atomic configuration of pristine carbon nanotubes (NTs) via the incorporation of heteroatoms (B, N or BN) or via the surface functionalization is a perfect way of control their opto-electronic properties [1-5]. However, it is worth noting that a very detailed analysis of this atomic configuration and concentration of the different species of these heteroatomic/functionalized nanotubes is highly required in order to determine their impact on the electronic/optoelectronic properties of the NTs. In this sense, transmission electron microscopy (TEM) is an essential tool to perform such studies [1-5]. In particular, spatially-resolved electron energy loss spectroscopy (SR-EELS), developed in an aberration-corrected TEM (having access to a close to 1 angstrom electron probe), is the most powerful technique to achieve these goals.

In this communication, we present a detailed study of the atomic configuration of different kinds of heteroatomic (CNx, BxCyNz) and functionalized single-walled NTs via SR- EELS [4-6]. We have examined the different chemical species present in the NTs, determined their average concentration as well as their spatial distribution within the walls and studied their chemical environment and bonding.

[1] R Arenal, X Blase, A Loiseau, Advances in Physics 59, 101 (2010)
[2] P Ayala, R Arenal, A Rubio, A Loiseau, T Pichler, Rev. Mod. Phys. 82, 1843 (2010)
[3] R Arenal, K March, C P Ewels, X Rocquefelte, M Kociak, A Loiseau, O Stéphan, Nano Lett. 14, 5509 (2014)
[4] R Wang, A Lopez-Bezanilla, A Masseboeuf, M Monthioux, R Arenal, Submitted
[5] R Arenal, L Alvarez, S Campidelli, R. Le Parc, J.-L. Bantignies, Submitted
[6] The research leading to these results has received funding from the EU under Grant Agreements 312483-ESTEEM2 and 604391 Graphene Flagship, from the Spanish Ministerio Economia y Competitividad (FIS2013-46159-C3-3-P) and from the EU under the Marie Curie Grant Agreement 642742 - Enabling Excellence

Grain boundary segregation of P in Ni-base alloy

J Tian, Y Chiu and I Jones

University of Birmingham, UK

The effect of P on the mechanical properties of Ni-base alloys is dramatic even with a low content due to its segregation to the grain boundaries. Thus a knowledge of grain boundary segregation is essential for a deep understanding of the effect of P on Ni-base alloys. Samples with a nominal composition of Ni-Al (6 at%)-P (0.1 at%) were prepared by arc melting and heat treated at 1300˚C for 48h. Recrystallization with a strain of 60% and heat treatment of 2h at 700˚C following by water quenching was utilized to optimize the grain size. The average grain size was measured by SEM-EBSD as 21μm (fig.1a). TEM samples were prepared by twin-jet polishing and examined on an FEI Talos equipped with 4 EDS detectors. Samples were carefully tilted until the projected grain boundary width was less than 2nm (fig.1b). An obvious P x-ray peak was detected in the spectrum from the grain boundary, while it was much weaker in the grain interior, indicating the existence of grain boundary P segregation (fig.1c). This is consistent with the line scan and mapping results shown in fig.1d-e. To reveal the relationship between grain misorientaion and P concentration at the grain boundaries, several grain boundaries were checked and at least three points were measured for each grain boundary. The misorientations were measured by calculating the normal direction of the foil by electron diffraction. With increasing misorientation, the P concentration increased

except for the twin boundary (fig.1f). This could be due to the concentration difference of the phosphorus-vacancy complexes between grain interior and grain boundary caused by the different configurations of grain boundaries with different misorientations.

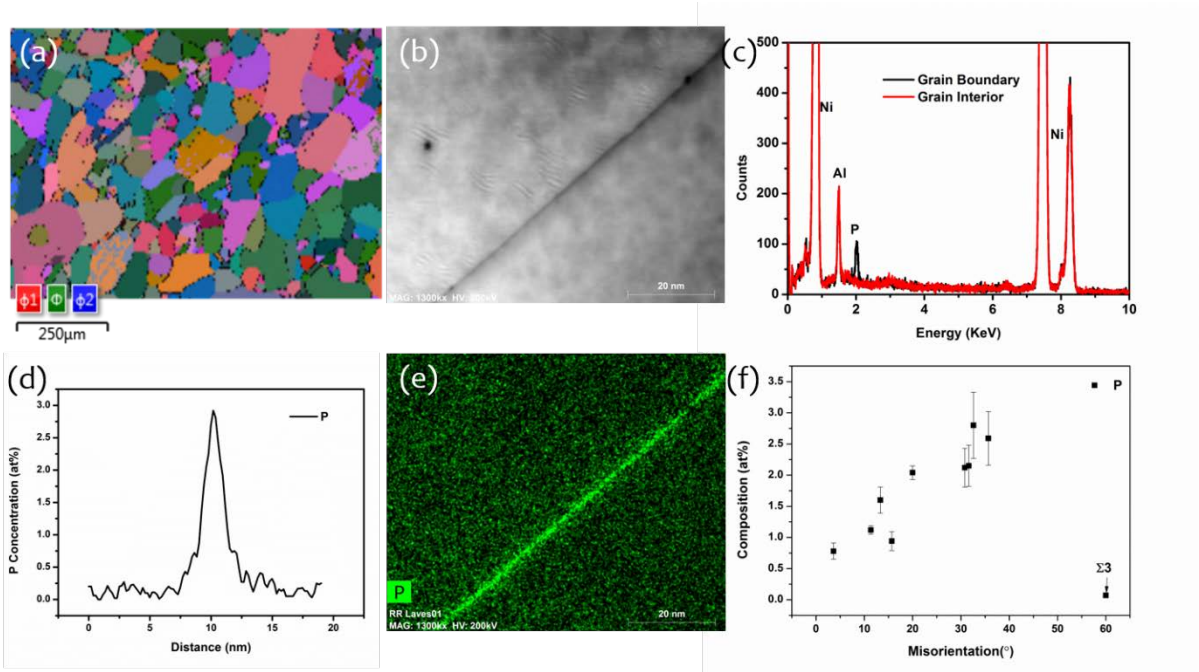

Figure 1. (a) EBSD orientation map of the recrystallized sample, (b) HAADF image of a typical grain boundary. (c) EDS spectra obtained at a grain boundary and in the grain interior, (d) line scan across a grain boundary, (e) EDS mapping results and (f) the relationship between grain misorientation and P concentration at grain boundaries.

ALCHEMI studies on Cr, Fe and Ni substitution in manganese cobaltite spinels

L V Gambino[1,3], N J Magdefrau[2] and M Aindow[1]

[1]University of Connecticut, USA, [2]United Technologies Research Center, USA, [3]Johnson Matthey, USA

The effects of Cr-, Ni- and Fe substitution into manganese cobaltite (MCO) spinels is of great interest due to the roles that the diffusion of these cations play in reaction layer development during high temperature exposure of MCO-coated alloys. Here we report a study on a series of model Cr-, Ni- and Fe-substituted MCO spinel ceramics produced by consolidation of combustion-synthesized oxide powders. The cation site occupancies in these samples have been studied by X-ray spectrometry-based Atom Location by CHanneling Enhanced MIcroanalysis (ALCHEMI) experiments in the transmission electron microscope, with the data being analyzed using the ordering tie line approach. In Cr-substituted samples, the Cr ions lie on the octahedral B sites and the Co ions reside on the tetrahedral A sites with Mn occupying the remaining sites. In Ni-substituted samples, all of the Ni ions occupy the B sites and the Co and Mn ions tend to lie on A and B sites, respectively. In contrast to the Cr-substituted samples, there is some mixing of the Co and Mn ions on the two types of sites at lower Ni contents. In Fe-substituted samples with lower Fe contents, all of the Mn ions occupy the B sites, roughly equal proportions of Fe ions occupy the A and B sites, and Co ions fill the remaining sites. With increasing Fe content, the degree of order decreases which ultimately results in the High Fe sample exhibiting no channeling evidence for preferred site occupation. These ALCHEMI data are compared with those obtained from reaction layers formed in MCO-coated Crofer 22APU. It is shown that the site occupancy preferences measured from the ceramic samples are also reflected in the reaction layers, and the consequences of these observations for the polaronic conductivity of these coated systems are discussed.

Is the electronic structure of few layer transition metal dichalcogenides always two dimensional?

J Yuan[1], J Hong[2], K Li[3], C Jin[2], X Zhang[2] and Z Zhang[2]

[1]University of York, UK, [2]Zhejiang University, China, [3]King Abdullah University of Science and Technology (KAUST), Saudi Arabia

The transition metal dichalcogenides (MoS_2 etc.) are a new class of layered materials that can be prepared in variable layer thickness down to single molecular layer. Compared with the more well-known graphene, the monolayer version of graphite, the transition metal dichalcogenides are semiconductors and hence can be more useful in applications such as light emission or photovoltaics where an energy gap is essential.

Ultra thin transition metal dichalcogenides also show interesting layer thickness dependent physical properties. For example, the semiconductor gap was found to change from indirect to direct when the layer thickness is reduced to monolayer, making monolayer MoS_2 an efficient light emitter.

Here we present investigation of the dimensionality of the joint density of states involved in the interband transition in MoS_2 using angle resolved electron energy loss spectroscopy [1]. To aid the analysis, we have extended the theory of joint density of states from three-dimensional semiconductors to low-dimensional semiconductors.

We show not only that the character of the interband transition changes from indirect to direct, as the layer thickness is reduced down to monolayer, as expected, but the indirect band gap retains a three dimension character down to the monolayer limit. This is compared with the two dimension character found for the direct bandgap transition in the monolayer MoSe and presumably also in MoS_2. Our result is consistent with the assumption made by Castellanos-Gomez et al. [2] when interpreting the electrostatic screening effect observed in monolayer MoS_2, which is very different from that of grapheme. Our result also can explain the sensitivity of the indirect interband transition as a function of the layer thickness and the bandgap cross-over of few layer MoS_2 from indirect to direct.

[1] J H Hong, K Li, C H Jin, X X Zhang, Z Zhang and J Yuan (2016) "Layer-dependent anisotropic electronic structures of freestanding quasi-two-dimensional MoS_2", Phys. Rev. B. (accepted)
[2] A Castellanos-Gomez et al. (2013), Adv. Mater. 25, 899-903

Friday 8 April

(Invited) Looking for the potential in digital large-angle electron diffraction patterns

R Beanland

University of Warwick, UK

The sensitivity of convergent beam electron diffraction (CBED) to a crystal's structure and electron density has been known for a long time. The technique has the advantage of sampling material limited only by the size of the electron beam and the thickness of the specimen, i.e. a volume that can easily be less than 5000 cubic nanometres. However, the small electron wavelength of high energy electrons leads to very small Bragg angles, which severely restricts the convergence angle that can be used. The problem becomes worse for materials with larger lattice parameters, often with the result that insufficient information is obtained from CBED to do anything useful.

Computer control of transmission electron microscopes and digital image capture allows hundreds, or thousands, of CBED patterns to be collected automatically. The patterns can then be combined to construct a single 'digital' large-angle convergent beam electron diffraction (D-LACBED) pattern that has no restrictions due to Bragg angle. These patterns have a wealth of detail and, for example, symmetry determination becomes straightforward. Examples are given from materials that would be difficult or impossible using conventional CBED.

While analysis of the intensities in CBED patterns has been shown to yield information about crystal potentials – even providing sufficient detail to show the redistribution of electrons between atoms (i.e. bonding effects) – there has been less work on LACBED patterns. Careful experimentation and energy filtered imaging is needed for CBED work, since reliable answers usually require elastically-scattered intensities to be measured with accuracies better than 1%. For D-LACBED patterns, it may be hoped that the large amount of data contains some regions that are much more sensitive than others. Thus, the sensitivity of D-LACBED patterns to changes in the crystal potential is investigated using Bloch wave simulations. It is found that dynamical diffraction effects often produce large changes in the intensity of multiple diffracted beams from the variation of a single Fourier coefficient that describes the crystal potential. It thus seems possible that highly accurate measurement of crystal structure and bonding on a routine basis is readily achievable with a modern computer controlled TEM without the need for energy filtering.

Quantitative comparison of phase contrast imaging in conventional TEM focal series and STEM ptychography

E Liberti[1], H Yang[2], G T Martinez[1], J S Kim[1], P D Nellist[1] and A I Kirkland[1]

[1]University of Oxford, UK, [2]Lawrence Berkeley National Laboratory, USA

In phase contrast imaging, three-dimensional, quantitative information about the specimen is encoded in the object wave function, which results from the interaction of the electron wave with the specimen potential. For weak scattering materials, such as mono-layer graphene, the phase of the object wave contains all the structural information. However, in the transmission electron microscope, this phase information is lost in the image recording process. In order to recover the phase, a variety of numerical reconstruction methods are available, including off-axis electron holography [1], focal series reconstruction [2] and ptychography [3]. To understand quantitatively materials properties', both matching of experimental phases is required, together with agreement with simulations. In practice, the quantitative information that is obtained from the experimental object wave is often in disagreement with image simulations, even for the simple case of a mono-atomic layer of graphene. This disagreement is in effect a phase mismatch, leading to an intensity mismatch also known as the Stobbs factor [4]. In this contribution, we focus on the comparison between conventional focal series phase restoration in transmission electron microscopy (TEM) and ptychographic phase restoration in scanning transmission electron microscopy (STEM) for the simple case of a mono-layer graphene. Both techniques restore the object wave phase with atomic resolution, and we explore the meaning of the measured phase through careful comparison of the experimental data recovered from

both techniques. We further examine the Stobbs factor for each case by comparison with imaging calculations, where we reproduce step by step the experimental restoration procedure. In this context, we will discuss the role of phonon scattering in the elastic scattering of graphene, as atomic thermal motion is considered to be one of the main causes underlying the Stobbs factor [5]. Further comparisons with simulations include analysis of the phase restored from focal series of TEM images under heating, as well the effects of using zero-loss filtered images to exclude inelastic scattering.

[1] M Lehmann, E. Völkl, F. Lenz, Ultramicroscopy 54 (1994) 335 – 344
[2] W M J Coene, A. Thust, A. Op de Beeck, D. Van Dyck, Ultramicroscopy 64 (1996) 109 – 135
[3] J M Rodenburg, B C McCallum, P D Nellist, Ultramicroscopy 48 (1993) 304 – 314
[4] M J Hÿtch, W M Stobbs, Ultramicroscopy 53 (1994) 191 – 203
[5] A Howie, Ultramicroscopy 98 (2004) 73 – 79. Acknowledgement The research leading to these results has received funding from the European Union Seventh Framework Programme under Grant Agreement 312483-ESTEEM2 (Integrated Infrastructure Initiative–I3)

Mapping the crystal morphology of graphene oxide with scanning electron diffraction

A S Eggeman, R K Leary and P A Midgley

University of Cambridge, UK

The current major interest in two-dimensional (2D) materials engenders need for techniques capable of mapping comprehensively their crystallographic landscapes. Here we show that scanning electron diffraction (SED) with versatile post-acquisition computational analysis can enable both the local atomic structure as well as the microstructure of 2D materials to be characterised in a rapid yet extremely information-rich manner. Computational interrogation of the four-dimensional SED datasets enables rigorous and intricate 'crystal cartography', making use of methods such as 'virtual' apertures and automated crystal orientation mapping. In this work we have applied SED to reveal the crystal morphology of few-layer graphene oxide. The SED approach significantly expands analytical capabilities, revealing intricacies of grain structure, grain boundaries, stacking arrangements and topography. We expect SED to contribute significantly to the comprehensive elucidation of a range of single- and few-layer 2D materials and composite-layered assemblies, providing a valuable tool for understanding their unique materials science and in determining properties of key importance for application in practical materials and devices.

STEM strain measurement from a stream of diffraction patterns recorded on a pixel-free delay-line detector

C Mahr[1], K Müller-Caspary[1], M Schowalter[1], A Oelsner[2], P Potapov[3] and A Rosenauer[1]

[1]Universität Bremen, Germany, [2]Surface Concept GmbH, Germany, [3]GLOBALFOUNDRIES, Germany

Recent progress in nano-beam electron diffraction, ptychography and differential phase contrast microscopy [1] is based on the acquisition of a four-dimensional data set I(xp,yp,x,y) with (xp,yp) the position of the STEM probe, (x,y) a coordinate in the recorded image/diffraction pattern and intensity I. Since the speed of conventional charge-coupled devices is limited, a major challenge is the development of fast detectors.

Here we present pilot experiments with a delay-line detector (DLD) mounted on an FEI Titan facility. Each electron impinging on the microchannel-plate stack of the DLD causes a cascade of secondary electrons. These electrons generate electrical pulses in two meandering wires. Depending on the incident position of the electron a characteristic time delay between the arrivals of the 2 conjunct pulses at the ends of each wire is measured, giving the coordinate of incidence perpendicular to the meander. By crossing two such delay-lines the point (x,y) and time τ of incidence can be detected and thus an image can be reconstructed.

We present strain measurements from convergent beam electron diffraction patterns [2] recorded at a STEM-raster of e.g. 100x100 pixels. Dwell times between 40 and 5ms have been used, corresponding to an acquisition of 10,000 diffraction patterns in 6.5 and 0.8min, respectively. In a GeSi-MOSFET we observe different strain regimes inside the GeSi-stressors owing to different Ge contents. Furthermore we show strain and rotation maps of catalytically interesting nanoporous gold, which has a sponge-like crystalline structure formed by the Au remaining from chemically corroded AuAg alloys.

Finally we show theoretical values [3] for precision and accuracy of the measured strain using nano-beam diffraction. As the precision of the measurement suffers from noise in the diffraction pattern, the precision degrades for shorter image integration times. On the other hand the precision can be increased using a precessing electron beam, as the diffraction discs are illuminated more homogeneously and hence their positions can be detected more precisely. In this way a compromise between precision and speed of the measurement has to be found.

[1] Nature Communications 5, 5653 (2014).
[2] Microscopy and Microanalysis 18, 995 (2012).
[3] Ultramicroscopy 158, 38 (2015).

Correlation of improved bioactivity of spray-pyrolysed glasses with structure from an electron diffraction study

Y-J Chou[1], K B Borisenko[1], S-J Shih[2] and A I Kirkland[1]

[1]University of Oxford, UK, [2]National Taiwan University of Science and Technology, Taiwan

Bioactive glasses have received considerable attention due to their superior bioactive properties and possible applications, including bone implants, drug carriers and sealant materials in dentistry [1]. Usually these glasses are prepared by melt quenching or sol-gel methods. However, it has been recently demonstrated that spray pyrolysis offers an effective one-step synthesis, which also improves bioactivity [2].

To understand the improved bioactivity building structure-property correlations of Nano volumes of material is an important step. Typically, amorphous materials are investigated by X-ray or neutron diffraction but due to the relatively large interaction volume for both of these probes, these techniques are not suitable for studying nanoscale variations in structure. However electron probes can be focused on specifically chosen nanoscale areas. The data from electron diffraction patterns can be transformed into a reduced density function (RDF) which describes the distribution of nearest-neighbour distances with high precision and can be used to build atomistic models of these materials [3].

In this study, we will report electron diffraction and RDF analyses to investigate the local structure of several spray-pyrolysed bioactive glasses with different composition. The results indicate that with decreasing Si concentration the bioactivity of the materials increases. We propose an atomistic structural model that correlates with the observed improvement in bioactivity, and discuss ways to design novel glass compositions with better bioactivity.

[1] L L Hench, Bioactive ceramics: theory and clinical applications, Bioceramics, 7 (1994) 3-14
[2] S-J Shih, Y-J Chou, I-C Chien, One-step synthesis of bioactive glass by spray pyrolysis, J Nanopart Res., 14 (2012) 1-8
[3] D J H Cockayne, The Study of Nanovolumes of Amorphous Materials Using Electron Scattering, Annu. Rev. Mater. Res., 37 (2007) 159-187

Session: Applications II

(Invited) Aberrated electron probes for magnetic spectroscopy with atomic resolution

J Rusz[1] and J-C Idrobo[2]

[1]Uppsala University, Sweden, [2]Oak Ridge National Laboratory, USA

Scanning transmission electron microscopes (STEM) with probe aberration correctors can today routinely provide detailed atomic resolution images, including spectroscopic information at every single pixel of the image, as the third dimension of the dataset. The shape of the electron energy loss spectrum carries a wealth of information about the element, its chemical state and local electronic structure. The latter was also shown to provide information about the magnetic properties of the atomic column via an effect called electron magnetic circular dichroism (EMCD; [1]), in analogy with its xray counterpart, where magnetic moments are measured via a difference of absorption of left- and right-handed circularly polarized x-rays.

In the last years, substantial effort was invested into high spatial resolution EMCD. This has been largely motivated by introduction of electron vortex beams (EVBs; [2,3,4]) into the world of transmission electron microscopy (TEM). It has been suggested that EVBs will allow measurement of EMCD directly at the transmitted beam [3].

Recently it was shown via a model and simulations on crystalline samples that this comes with a requirement of an atomic size probe, otherwise the vortex phase distribution in the electron beam would not be effective and, as a consequence, the EMCD at the transmitted beam direction would vanish [5]. In addition, it was suggested that EMCD can be measured by tuning the phase distribution of an electron beam to the underlying crystal structure of the specimen [6]. Desired phase distributions should be achievable by setting nonzero aberrations of specific symmetry, as dictated by crystal structure of the sample.

Here, we develop this idea further and describe methods for detection of out-of-plane and also in-plane magnetization, utilizing atomic size electron probes. We describe astigmatic probes for a range of lattice parameters optimized for the largest signal to noise ratio. We will discuss various direction to further optimize the magnetic signal strength via shaping the apertures and/or manipulating the phase of the probe in more general ways.

[1] P Schattschneider et al., Nature 441, 486 (2006).
[2] M Uchida, and A Tonomura, Nature 464, 737 (2010).
[3] J Verbeeck, H Tian, and P Schattschneider, Nature 467, 301 (2010).
[4] B McMorran et al., Science 331, 192 (2011).
[5] J Rusz, and S Bhowmick, Phys. Rev. Lett. 111, 105504 (2013).
[6] J Rusz, J C Idrobo, and S Bhowmick, Phys. Rev. Lett. 113, 145501 (2014).

In-situ formation study and oxidation of Fe nanoparticles in an aberration corrected E-(S)TEM

L Lari, R Carpenter, V K Lazarov, E D Boyes and P L Gai

University of York, UK

Fe and Fe-oxide nanoparticles have a series of promising potential applications in physical and medical sciences. These include magnetic storage devices, catalysis, sensing, contrast enhancement in magnetic resonance imaging and magnetic hyperthermia [1-3].

Understanding of the Fe-Oxide NPs reduction to metal and the oxidation processes down to atomic scale is paramount for the control of the quality and the optimization of their applications.

A recently modified double aberration corrected JEOL 2200FS (S)TEM [4] has demonstrated the possibility of the analysis of metallic nanoparticles in gas environment at temperature allowing single atom visualisation by HAADF STEM in controlled gas reaction environment [5].

In this study, thin films of were deposited by sputtering on C films supported by standard TEM Cu grids. Nanoparticles were produced by annealing in-vacuum within the microscope column pre-sputtered iron thin films.

Nanoparticle formation and size distribution was monitored in-situ as a function of time and temperature by HAADF STEM imaging. After annealing nanoparticles were shown to consist of single crystal metallic Fe, composition confirmed by EDX analysis.

The oxidation of the Fe nanoparticles was then studied in-situ. The interaction of the nanoparticles with the gas, will be discussed in terms of the changes in nanoparticle geometry, composition, size distribution, crystallinity and microstructural defects.

[1] B D Terris and T Thomson, J. Phys. D 38, R199–R222 (2005)
[2] H Galvis et al. Science 335, 835–838 (2012)
[3] Q A Pankhurst, N T K Thanh, S K Jones, and J Dobson, J. Phys. D 42, 224001 (2009)
[4] P L Gai and E D Boyes, Microscopy Research and Technique 72, 153 (2009)
[5] E D Boyes, M R Ward, L Lari, and P L Gai, Annalen der Physik 525, 423 (2013)

3D ion beam tomography of nickel-base superalloys for morphological and spatial analysis

S A Croxall, R Krakow and P A Midgley

University of Cambridge, UK

Nickel-base superalloys are aerospace materials that exhibit exceptional mechanical properties and corrosion resistance at very high temperatures. RR1000 is used in discs in gas turbine engines, where temperatures reach in excess of 650°C with high mechanical stresses. Study of the microstructure at the micron and sub-micron level has conventionally been undertaken using scanning electron microscope images, and whilst this provides 2D information of the revealed surface, the underlying 3D microstructure can be inferred only with additional knowledge. Using a dual-beam workstation (FEI Helios Nanolab 600), we are able to interrogate directly the 3D microstructure using a serial sectioning (slice and view) approach.

Using the ion beam for the imaging step of the serial sectioning routine can produce good compositional contrast based on the ionisation energies of the constituent elements of the superalloys. This was first applied to the γ' precipitate microstructure of RR1000 producing 3D reconstructions for a range of differently heat treated samples. Using the acquired data we were able to compare 2D and 3D measurements in order to validate the 3D technique, as well as highlight potential problems with 2D characterisation. Size and spatial distributions showed differences between the different samples, whilst surface area to volume ratios showed variations in the shape of the γ' precipitates depending on their size.

3D data sets were also obtained of the η phase of the superalloy ATI 718Plus, enabling comparisons between two regions of a turbine disc. The 3D reconstructions allowed for the full range of η precipitate morphologies to be assessed, showing the interactions between the individual precipitates and the grain structure of the alloy. Spatial analysis enabled a quantitative comparison between the two samples in terms of the η precipitate spacing and relative orientation, giving insight into differences in mechanical performance between the two samples.

Session: Applications II (continued)

Revealing local polarisation and domain configurations in ultrathin ferroelectric tunnel junctions by annular bright field STEM

J J P Peters, G Apachitei, R Beanland, M Alexe and A M Sanchez

University of Warwick, UK

High-quality ultrathin ferroelectric films down to 3 unit cells [1] have been recently achieved, reinvigorating the use of oxides in non-volatile memory cells using polarisation orientation to encode binary values. Ferroelectric domain walls are also expect expected to alter the functional properties of the system, including electronic conduction and ferromagnetism, forming a new type of 2D functional nanomaterials [2]. Density of potential devices will then depend on the width of the domains and domain walls, previously shown to be drastically altered by the film thickness and boundary conditions.

A popular device is the multiferroic tunnel junction, consisting of an ultrathin ferroelectric dielectric between two different ferromagnetic electrodes in a capacitor configuration. This forms a novel 4- state memory device where a tunnelling current between the electrodes depends on the electrode magnetisation orientation as well as the polarisation direction of the dielectric [3]. In these small devices it is crucial to have an understanding of the polarisation at the unit cell level. However, previous experimental studies at such scales have largely focussed on devices with insulating electrodes, unsuitable for an electronic device.

Using aberration-free scanning transmission electron microscopy (STEM), we analysed in detail the domain configuration of a real ferroelectric tunnel junction with asymmetric depolarising fields. Here, ultrathin ferroelectric $PbTiO_3$ films were used as the barrier between ferromagnetic Co and $La_{0.7}Sr_{0.3}Mn_{03}$ electrodes. $PbTiO_3$ of 9, 6 and 3 unit cells thick were examined using annular bright field imaging to measure the positions of all atom types, revealing the local polarisation and hence the domain pattern [4]. For the given system with a set lattice strain, the depolarization field becomes relatively large with smaller film thickness and has a clear influence on the equilibrium domain pattern. The measured dipole distribution reveals the evolution from conventional 180° Kittel type domains to flux closure Landau-Lifshitz and vortex type domain configurations with reduced film thickness.

[1] Fong, D D et al. Ferroelectricity in Ultrathin Perovskite Films. Science 304, 1650–1653 (2004).
[2] Catalan, G, Seidel, J, Ramesh, R & Scott, J F Domain wall nanoelectronics. Rev. Mod. Phys. 84, 119–156 (2012).
[3] Pantel, D, Goetze, S, Hesse, D & Alexe, M Reversible electrical switching of spin polarization in multiferroic tunnel junctions. Nat Mater 11, 289–293 (2012).
[4] Jia, C-L et al. Unit-cell scale mapping of ferroelectricity and tetragonality in epitaxial ultrathin ferroelectric films. Nat Mater 6, 64–69 (2007).

Advances towards 2D and 3D quantitative STEM-EDX

T Slater[1], S Haigh[1] and N Zaluzec[2]

[1]University of Manchester, UK, [2]Argonne National Laboratory, USA

We present recent advances towards two dimensional (2D) and three dimensional (3D) quantitative energy dispersive X-ray (EDX) spectroscopy in the scanning transmission electron microscope (STEM). This includes examination of X-ray absorption in spherical nanoparticles for accurate elemental quantification and development of best practices for 3D chemical mapping using STEM-EDX tomography.

Recent developments in energy dispersive X-ray (EDX) detector design have renewed interest in 2D and 3D STEM-EDX spectrum imaging due to much higher available X-ray count rates [1,2], including elemental mapping of nanoparticles [3] . STEM-EDX spectrum imaging can be combined with electron tomography in order to provide 3D elemental maps at nanometre resolution [4,5]. Here, the considerations needed to perform accurate STEM-EDX tomography are discussed, with consideration of detector shadowing and X-ray absorption [6]. The use of a time-varied acquisition scheme is shown to greatly increase the fidelity of certain STEM-EDX reconstructions [6].

Additionally, X-ray absorption through nanoparticles of spherical geometry is presented in order to provide accurate X-ray absorption correction in 2D spectrum images of nanoparticles. A novel correction scheme is proposed that is shown to account for X-ray absorption in Au nanoparticles of diameters between 5 – 400 nm [7] . Absorption correction is then extended to 3D geometries through the calculation of 3D absorption correction factor matrices derived through quantification from STEM-EDX tomography.

[1] von Harrach, H S et al. Microscopy and Microanalysis 15, 208-209 (2009).
[2] Zaluzec, N J Microscopy and Microanalysis 19, 1262-1263 (2013).
[3] MacArthur, K E et al. 'Quantitative Energy-Dispersive X-Ray Analysis of Catalyst Nanoparticles Using a Partial Cross Section Approach', Microscopy and Microanalysis In Press.
[4] Genc, A. et al. Ultramicroscopy 131, 24-32 (2013).
[5] Slater, T. J. A. et al. Nano Letters 14, 1921-1926 (2014).
[6] Slater, T. J. A. et al. Ultramicroscopy 162, 61-73 (2016).
[7] Slater, T. J. A. et al. 'X-Ray Absorption Correction for Quantitative STEM-EDX of Spherical Nanoparticles', Microscopy and Microanalysis Accepted.

(Plenary) Advances in EELS for materials research

A J Craven

University of Glasgow, UK

Over the last two decades or so there have been major advances in electron optics leading to sub-Ångstrom spatial resolution in STEM and ~10meV energy resolution in EELS. To achieve these improvements in "headline" performance, there have had to be major improvements in instrumental stability, the factor that often limits what can be achieved in practice. In addition, there have been major advances in data collection, data processing and data interpretation. As a result, the power of STEM-EELS for materials research has grown enormously.

These improvements will be reviewed briefly. The physics of the energy loss processes relevant to EELS will also be reviewed. Examples will be given showing how the various improvements have benefitted (or have the potential to benefit) materials research.

Finally some recent work on measurements of both absolute inelastic mean free paths and differential cross-sections for core losses will be described and their application to the analysis of precipitates in steels will be discussed.

Posters

P:01 (Flash presentation) Recent developments in ptychography using a fast pixelated detector in the scanning transmission electron microscope

G T Martinez[1], H Yang[2], L Jones[1] and P D Nellist[1]

[1]University of Oxford, UK, [2]Lawrence Berkeley National Laboratory, USA

The use of fast pixelated detectors (FPD) fitted to the scanning transmission electron microscope (STEM) is gaining considerable attention due to the possibility to record the full convergent beam electron diffraction (CBED) pattern for each probe position that is scanned over the sample. This results in a 4D–dataset (2D CBED – 2D image scan) that contains all the scattering information from the STEM experiment. When using ptychography reconstruction methods [1,2], the analysis of this 4D–dataset allows the retrieval of the wave phase variation due to the interaction with the specimen's potential. Previous work has shown an experimental demonstration of efficient phase contrast imaging at atomic resolution using this technique [3], as well as a discussion on the optimal imaging conditions based on theory and simulations [4].

In this work, we further present the possibilities of materials structure determination when using a FPD in the STEM. We compare and discuss the use of different phase reconstruction algorithms, such as the Single Side Band (SSB) [2, 3] and the Wigner- Distribution Deconvolution (WDD) methods [1]. Furthermore, the ptychography methods allow for an estimation of the probe profile interacting with the sample, which is useful to determine the probe aberrations during the experiment and correct for them in the reconstructed image. By doing this, high resolution atomically resolved phase images of light elements can be obtained, which would not be possible to get using conventional techniques [5]. Moreover, an optical sectioning effect is observed when deconvolving with different probe functions [5]. Finally, we explore the robustness of this technique to dynamical effects using multislice simulations.

[1] J M Rodenburg and R H Bates, Phil. Trans. R. Soc. Lond. A. 339 (1992) 521 – 553.
[2] J M Rodenburg, B C McCallum, P D Nellist, Ultramicroscopy 48 (1993) 304 – 314.
[3] T J Pennycook, A R Lupini, H Yang, M F Murfitt, L Jones, P D Nellist, Ultramicroscopy 151 (2015) 160 – 167.
[4] H Yang, T J Pennycook, P D Nellist, Ultramicroscopy 151 (2015) 232 – 239.
[5] H Yang, R N Rutte, L Jones, M Simson, R Sagawa, H Ryll, M Huth, T J Pennycook,H Soltau, Y Kondo, B D Davis, P D Nellist, *manuscript submitted.*

P:02 (Flash presentation) Effects of instrument imperfections on quantitative scanning transission electron microscopy

M Schowalter, F F Krause, T Grieb, K Müller-Caspary, T Mehrtens and A Rosenauer

Universität Bremen, Germany

Quantitative scanning transmission electron microscopy nowadays is a standard tool for structural and chemical analysis. Direct comparison of experimental data with simulations is possible, if raw intensities are normalized with respect to the incoming beam intensity [1]. The incoming beam intensity can be measured by recording a detector scan. However, the detector is not perfect, but exhibits non-spherical shape and non-uniform sensitivity, that need to be taken into account [1,2].

In this contribution, we identify further imperfections and characterize how they affect quantitative STEM measurements. Investigated imperfections are inaccurate centering of the ronchigram and anisotropy of the detector sensitivity, the diffraction cut-off and distortions due to an image corrector, the sensitivity enhancement from an previous illumination, errors in the measured offset intensity due to the long afterglow of the detector and due to accidental electrons [3,4]. It was found that the most severe effect for quantitative STEM is due to distortions of

the diffraction pattern caused by an image corrector. Therefore, the conventional detector scan procedure, where the electron beam is scanned over the detector in image mode, needs to be replaced by a procedure, where the beam is rastered over the detector using a series of beam tilts in image mode. In this way, an effective sensitivity can be computed that accounts for the inhomogeneity of the detector as well as distortions and cut-off of the diffraction pattern.

Errors in offset intensity due to long afterglow and accidential electrons may be severe in atom counting in materials with low atomic number. An error of about 2.3 nm for 5 nm thick Si was found for the quantification of the specimen thickness.

[1] J M LeBeau, S Stemmer, Ultramicroscopy 108 (2008) 1653.
[2] A Rosenauer, et al., Ultramicroscopy 111 (2011), 1316
[3] R Ishikawa, et al., Microsc. Microanal. 20 (2014) 99.
[4] F F Krause et al., Ultramicroscopy 161 (2016), 146

P:03 (Flash presentation) The effect of oxygen on the contrast of ADF-STEM images

A Mostaed, G Balakrishnan, M R Lees and R Beanland

University of Warwick, UK

In the present work, we employ aberration-corrected scanning transmission electron microscopy (ac-STEM) to investigate the atomic structure of the quantum spin-ice Pyrochlore $Yb_2Ti_2O_7$ (YTO), using annular dark field (ADF) images. Images were taken along the [211] zone axis in which there are four types of heavy atom column (Fig. 1); those containing only Yb, those containing only Ti, and mixed (M) columns containing 50% Ti and 50% Yb. The distribution of oxygen atoms near to M columns is different for each (111) Kagome layer, leading to a further distinction that can be made between 50:50 columns in the Yb Kagome layer (M1) and 50:50 columns in the Ti Kagome layer (M2). There are twice as many oxygen atoms around M1 columns in comparison with M2; in this projection the oxygen atoms are ~72 pm from the M1 columns while those next to M2 columns lie at a distance of ~49 pm. The obtained results from both experimental and simulated ADF images (Fig. 1) showed a subtle difference in the intensity distribution around the mixed Ti/Yb columns, which is as a consequence of differences in oxygen atom positions. Thus, we show that the detailed intensity distribution around the visible atomic columns in the ADF-STEM images is sensitive to the presence of nearby atoms of low atomic number (in this case oxygen), even though they are not directly visible in the images. To the best of our knowledge, this is the first time that oxygen columns with a distance of ~30 pm have been detected in ADF-STEM images.

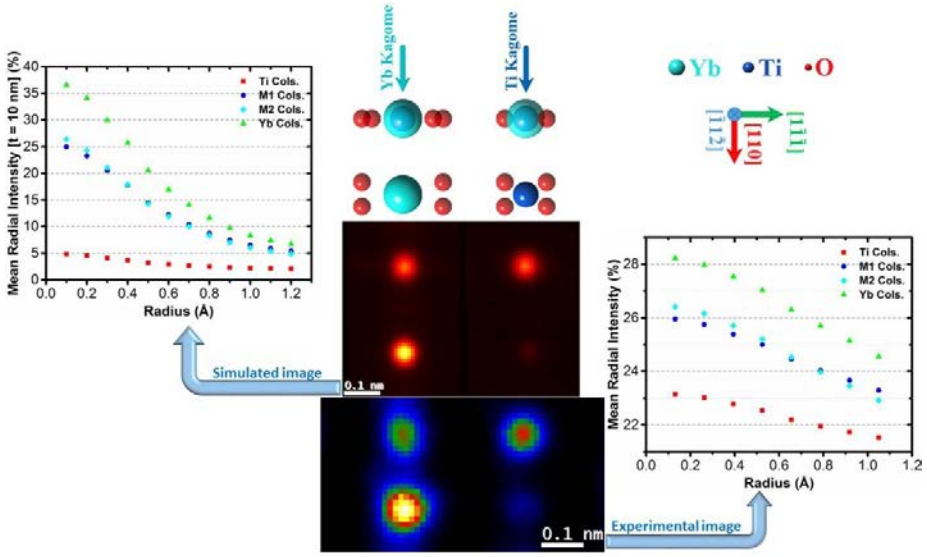

Fig. 1. [211] ADF-STEM image of YTO with overlaid Yb, Ti and M columns. The presented plots show the intensity distribution around the atomic columns for the experimental and simulated images.

P:04 (Flash presentation) Time-resolved imaging and analysis of single atom diffusion on graphene oxide

T Furnival[1], R Leary[1], E C Tyo[2], S Vajda[2], J M Thomas[1], P D Bristowe[1] and P A Midgley[1]

[1]University of Cambridge, UK, [2]Argonne National Laboratory, USA

Single atoms and small atomic clusters offer a range of novel, tunable properties for a number of applications such as selective catalysts [1]. Achieving precise control of the desired properties of these systems first requires an understanding of the interaction between the cluster and its support. Advances in aberration-corrected scanning transmission electron microscopy (STEM) mean that atomic resolution imaging and characterisation is now achievable for many materials. Observing individual atoms and small clusters remains difficult, however, due to low signal-to-noise ratio and beam-induced motions causing blurring during image acquisition. One route around these problems is to acquire rapid image sequences in an effort to reduce the electron dose and also capture any dynamic behaviour of the atoms. Exploiting the spatial and temporal correlations between frames, and using a novel processing method based on singular value thresholding [2], we have developed robust approaches to recover individual atomic positions, including STEM acquisition rates of 10 frames per second or better [3].

We have applied the approach to the study of catalytically important copper, as well as other atoms, on few-layer graphene oxide (GO), where the presence of functional groups on GO may aid the control of deposited clusters by acting as preferential pinning sites. Analysis of an annular dark-field STEM image sequence reveals a range of behaviours, with some stronglypinned atoms and other more mobile atoms undertaking random walks on the surface. Further investigation of the atom trajectories uncovers preferred jump lengths and directions in agreement with discrete sites on a graphene-like lattice. Combined with ab-initio DFT calculations, this analysis provides a new insight into the formation and behaviour of small atom clusters under an electron beam, and the interactions between few-atom catalysts and high surface area supports.

[1] Tyo, EC, Vajda, S (2015). Catalysis by clusters with precise numbers of atoms. Nat. Nanotechnol. 10, 577-588.
[2] Candes EJ, Sing-Long CA, Trzasko JD. (2013). Unbiased Risk Estimates for Singular Value Thresholding and Spectral Estimators. IEEE Trans. Signal Process. 61, 4643-4657
[3] Furnival T, Leary R, Midgley PA. (2016). Denoising microscopy image sequences with singular value thresholding. Manuscript in preparation

P:05 (Flash presentation) Angle-resolved scanning transmission electron microscopy employing an iris aperture

K Müller-Caspary[1], O Oppermann[1], T Grieb[1], A Rosenauer[1], F Krause[1], M Schowalter[1], T Mehrtens[1], P Potapov[2], A Beyer[3] and K Volz[3]

[1]Universität Bremen, Germany, [2]GLOBALFOUNDRIES, Germany, [3]Philipps-Universität Marburg, Germany

By commonly using a ring-shaped detector in annular dark field (ADF) scanning transmission electron microscopy (STEM), the technique exhibits total insensitivity to the angular distribution of scattered intensity within the detector ring. Here we report on angleresolved STEM (ARSTEM) which is capable of densely sampling the scattered intensity in dependence of the scattering angle. To this end, we developed a prototype iris aperture situated above the ADF-STEM detector in a Titan microscope. The radius of this aperture can be adjusted by a gear wheel driven by a stepper motor, which is controlled by the microscope acquisition software. A STEM image corresponding to an angle interval $\beta=[\beta1, \beta2]$ is obtained from $I(\beta)=I(\beta2)-I(\beta1)$ with images $I(\beta1,2)$ taken at iris radii $\beta1$ and $\beta2$. This system was preferred to ultrafast cameras due to their limited performance concerning dynamic range, radiation hardness

and the maximum spatial sampling rates in the STEM image. It furthermore reduces acquired data to a managable amount and allows simultaneous electron spectroscopy at low scattering angles.

We first demonstrate the independent quantification of specimen thickness and chemical composition in a GaN3%As97% layer embedded in GaAs using 2 STEM images formed by angular intervals [40,80] and [100,140] mrad. This enhances quantitative STEM analysis of nanostructures because the common interpolation of thickness in the layer is avoided, which can introduce inaccuracies in case of preferential etching or if regions with known thickness are too far away or not present at all. The result is discussed in terms of the scattering characteristics owing to Huang scattering, Z- and thickness contrast. Second, we investigate the angular scattering characteristics of a GeSi/Si-based field effect transistor with respect to strain-, thickness- and composition-dependent contrast in 32 images formed at different acceptance angles between 16 and 255mrad. The ARSTEM data is found to be consistent with multislice simulations for angles above 30mrad taking into account static and thermal disorder, whereas deviations at lower angles are discussed in terms of inelastic scattering and contamination. The Ge contents of 22% and 37% have been confirmed by conventional high-angle ADF-STEM and energy-dispersive X-ray analysis employing the chemiSTEM system.

P:06 (Flash presentation) Quantitative analysis of damage mechanisms in pharmaceutical materials by transmission electron microscopy

J Cattle[1], M S'ari[1], N Wilkinson[2], N Hondow[1], A Brown[1] and R Brydson[1]

[1]University of Leeds, UK, [2]Gatan UK, UK

Modern electron microscopy (EM) techniques and hardware offer some of the highest attainable spatial resolutions, making EM one of the best tools for microstructural analysis of a wide variety of materials. Organic materials, specifically pharmaceuticals, for which microstructure is a key part of their functionality would make ideal candidates for EM analysis, as it could provide useful feedback at various stages during drug development to check the presence of desired crystalline polymorphs, assess mixing quality, quantify crystal lattice defects and identify contamination. However, the major drawback to the use of EM is the high sensitivity of organic crystalline materials to electron beam exposure. Employing fluence rates that are typically used for inorganic samples would destroy all traces of crystallinity in most pharmaceutical materials [1]. Low-dose techniques have been used for many years to analyse beam sensitive samples [2] using EM, but with recent improvements in CCD camera sensitivities, microscope stabilisation and current control, combined with existing low-dose techniques, there is great opportunity for EM to be used for detailed organic materials analysis. Initially, the limits and flexibility of low-dose techniques need to be tested and documented, both qualitatively and quantitatively. From this, a deeper understanding of the damage mechanisms at play can be drawn out, informing on the limits of organic crystalline materials analysis by EM and indicating appropriate damage mitigation strategies which could be employed in future studies.

The changes in sample lifetime under differing microscope and sample conditions allows us to make suggestions as to the mechanisms of damage occurring. In this study, low-dose EM conditions were used to analyse the model organic crystalline material theophylline. The initial conditions used were: 200 kV electron beam accelerating voltage, electron fluence rates of 0.1 to 1 $e^-/Å^2/s$ and with the sample at room temperature. By making changes to various conditions (such as temperature, electron beam accelerating voltage and sample support substrate) and re-measuring the critical dose, we can discuss what these changes mean on a molecular level and what damage mechanisms and beam-sample interactions are responsible for the decaying of the sample structure. Additionally, by using the critical doses (CD) acquired during analysis at different temperatures, the activation energy for electron beam damage of theophylline has been calculated by using the Arrhenius equation and ln(1/CD) as the rate coefficient. This technique will then be repeated for a number of different, similarly sensitive, organic samples to establish the limits of EM analysis of sensitive organics.

[1] M S'ari, J Cattle, N Hondow, H Blade, S Cosgrove, RMD Brydson, AP Brown, 'Analysis of Electron Beam Damage of Crystalline Pharmaceutical Materials by Transmission Electron Microscopy', *J ournal of Physics: Conference Series*, 644, 1 – 5, (2015)
[2] DT Grubb, 'Radiation Damage and Electron Microscopy of Organic Polymers', *Journal of Materials Science*, 9, 1715 – 1736, (1974)

P:07 (Flash presentation) Ultrafast nano-fabrication and analysis using Xe plasma ion FIB-SEM microscope

A Benkouider[1], D Rai[2], S Sharang[1], T Hrnčíř[1], A Delobbe[3], M Rommel[4], J Oboňa[1] and J Jiruše[1]

[1]Tescan, Czech Republic, [2]University of Erlangen-Nuremberg, Germany, [3]Orsay Physics, France, [4]Fraunhofer Institut für Integrierte Systeme und Bauelementetechnologie IISB, Germany

The focused ion beam (FIB) technology combined with ultra-high-resolution scanning electron microscope (UHR-SEM) has become an increasingly popular tool for the fabrication, analysis and characterization for both scientific and industrial communities. Conventional FIB instruments are commonly based on Ga liquid metal ion source (LMIS). However, even if Ga LMIS has a reasonable resolution (typically up to 2.5 nm), Ga FIB instruments present some limitations. These include Ga ion implantation and contamination, formation of intermetallic compounds, slow sputtering rate and low secondary ionization coefficient. New liquid metal alloy ion sources (LMAIS) have been developed to overcome these limits; for example Au ions can be used for higher sputtering rate and Si ions are not acting as dopant in Si samples [1]. However, none of the proposed LMAIS sources is suitable for rapid milling because they can only deliver probe current up to few tens of nA (about 65 nA). Contrary, emerging Xe plasma FIB systems promise faster removal rates [2-3].

Here we show that a new Xe plasma FIB offers sputtering speed up to 50 times faster than the most powerful Ga FIBs. Compared to conventional Ga ion sources, the Xe plasma ion source reduces dramatically the time for cross-sectioning from tens of hours or even days to a matter of hours [4-5]. Moreover, combining this FIB column with an UHR-SEM column expands even more the advantages for such a tool by opening possibilities of ultra-fast 3D tomography, large TEM lamella preparation, failure analysis and surface preparation. The UHR-SEM sample observations during the milling process offers imaging of the resulting cross-section and EDX or EBSD analysis, all being integrated in the same instrument, thus enabling the creation of complex automated tasks. Furthermore, we show how to produce a very large cross-sections (longer than 150 µm) on pre-patterned substrates that are used further for EDX and surface analysis.

[1] A Benkouider et al, Thin Solid Films 543 (2013) 69-73
[2] T Hrnčíř et al, 38th ISTFA Proceedings (2012) 26
[3] J Jiruše et al, Microsc. and Microanal. 21 (2015) 1995
[4] A Delobbe et al, Microsc. and Microanal. 20 (2014) 298 [5] T. Hrnčíř et al, 40th ISTFA Proceedings (2014) 136

P:08 (Flash presentation) Dispersed graphite and graphene nanoflakes in mesoporous carbon

L Lari, Z Nedelkoski, V Budarin, J Clark and V Lazarov

University of York, UK

Starbon®, a family of mesoporous carbonaceous materials was recently developed at the University of York from polysaccharides (*e.g.* starch) [1-2]. The novelty and the advantages of these materials include cheap, green and renewable sources, low temperature carbonization processing, avoidance of harmful chemicals, and a tunability of the surface functionality from hydrophilic to hydrophobic. These properties make Starbon® an ideal candidate for applications in catalysis and material absorption [3].

Recently the tunability of the properties of these materials has been successfully extended to their functional properties by ball-mixing it with graphite and graphene before the carbonization process.

Here we present an Electron Microscopy study of these enhanced composite materials, by combining Electron Diffraction, Electron Energy Loss Spectroscopy and Aberration Corrected TEM/STEM Imaging in correlation with the physical and transport properties exhibited by the materials.

[1] P S Shuttleworth, A Matharu, J H Clark, in Polysaccharide Building Blocks, John Wiley & Sons, Inc., 2012, pp. 271-285
[2] V Budarin, J H Clark, J J E Hardy, R Luque, K Milkowski, S J Tavener, A J Wilson, Angew. Chem.-Int. Edit. 2006, 45, 3782-3786
[3] R J White, V Budarin, R Luque, J H Clark, D J Macquarrie, Chem. Soc. Rev. 2009, 38, 3401- 3418

P:09 (Flash presentation) Structural and spectroscopic analysis of Mn doped Bi_2Te_3

A Ghasemi[1], D Kepaptsoglou[2], L J Collins-McIntyre[3], A I Figueroa[4], L Lari[1], Q Ramasse[2], G van der Laan[4], T Hesjedal[3] and V K Lazarov[1]

[1]University of York, UK, [2]SuperSTEM Laboratory, UK, [3]University of Oxford, UK, [4]Magnetic Spectroscopy Group, UK

Three-dimensional topological insulators (3D-TIs) are a new class of materials with promising properties for fundamental physics as well as upcoming technological applications for spintronic devices. TIs are insulating in their bulk, however their surface states are gapless and protected by time-reversal symmetry (TRS) which makes them immune to surface impurities and backscattering. Doping of TIs with magnetic elements such as Mn should enable the control and opening of their surface band gap, and provides material platform for realisation of Quantum Anomalous Hall effect [1]. In this work by using TEM and STEM/EELS we systematically study the structure and chemical composition of Mn-doped Bi_2Te_3 grown by molecular beam epitaxy on Al_2O_3 (0001) substrate. The Bi_2Te_3 films were epitaxially grown and the STEM/EELS and EDX results show presence of Mn dopants at different sites of Bi_2Te_3 lattice. These results indicate that the local environment of the Mn atoms in the Bi_2Te_3 thin film is heterogeneous. To further investigate, we performed XANES and EXAFS experiments which their results confirm that Mn atoms can substitute in the Bi sites, interstitial in the van der Waals gap, as well as part of the MnTe compound. Moreover by employing GPA we show that the presence of Mn in the Van der Waals gap results in having strain in the Bi_2Te_3 lattice.

[1] Zhang, J-M, et al., Stability, electronic, and magnetic properties of the magnetically doped topological insulators Bi2Se3, Bi2Te3 ,and Sb2Te3. Physical Review B, 2013. 88(23): p. 235131

P:10 (Flash presentation) Size distribution investigations of thiol-stabilised silver nanoparticles

J A Watts, A la Torre, M W Fay, A N Khlobystov and P D Brown

University of Nottingham, UK

Ag nanoparticles (NP) may be regarded as generic building blocks for a range of nanostructured processes and there is particular interest in the control of their size and size distribution. Here, we report on the development of Ag NP synthesised using a modified Brust-Schiffrin reduction, and the effect of thiol addition on their size and distribution at the sample dispersion stage on to the TEM support grid. A solution of silver nitrate in ethanol, dodecanethiol, 11-(1Hpyrrol-1-yl)undecane-1-thiol and sodium borohydride, stirred for 2 h and then frozen, washed, filtered and dried produced a product of Ag NP. The product was dispersed in cyclohexane, with and without dodecanethiol, and drop cast onto a holey carbon / Cu TEM sample grid. Samples were observed in a JEOL 2100F TEM, operating at 200kV. The final processing step had a significant effect of the NP size distribution and dispersion. Samples dispersed from cyclohexane showed a biomodal size distribution (4,1.5nm) (Figure 1a). Conversely, samples dispersed from cyclohexane in the presence of dodecanethiol showed a much narrower, single size distribution (3,0.6nm) and a high level of self-assembly (Figure 1b). The fundamental differences in size distribution of the Ag NP product may be explained in terms of the combined effects of thiol on the colloidal suspension and solvent drying.

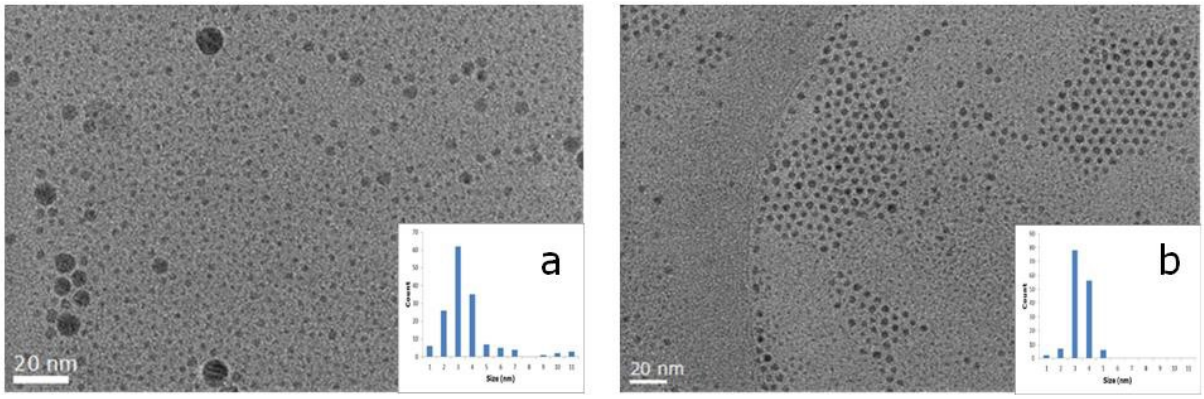

Figure 1 (a) Ag NP dispersed from cyclohexane; (b) Ag NP dispersed from cyclohexane in the presence of dodecanethiol.

P:11 (Flash presentation) Direct observation of in-situ sublimation of tellurium nanowires

S Marks[1], D Smith[2], D Cook[2], R Beanland[1] and J Sloan[1]

[1]University of Warwick, UK, [2]University of Southampton, UK

Sublimation is the direct phase transition from solid to gas without passing through an intermediate liquid phase. This phase transition is important as it becomes a lot more relevant when working under vacuum and can easily be confused with melting. Sublimation can be directly observed in-situ through the combination of ultra-high vacuum (UHV) and a sample heating holder. A material will sublime if its vapor pressure is equal to or greater than the partial pressure of the system. UHV is required for transmission electron microscopy (TEM), with the typical pressure inside a TEM being 5x10-7 mmHg. Therefore at this low pressure the vapor pressure of a material can become greater than or equal to the partial pressure inside the TEM if the sample is heated and sublimation can occur [1]. Tellurium nanowires were grown via Super Critical Fluid Electrodeposition [2] (SCFED) into porous anodic alumina templates with a range of diameters from 13-150nm. To allow for easy imaging the template is etched from the nanowires and they are drop cast onto a lacey carbon grid. The tellurium nanowires were identified to have a uniform growth orientation, the crystal plane parallel to the growth direction, of [001]. The sample was observed in

a JEOL 2100 TEM with an accelerating voltage of 200kV. The sublimation experiments are undertaken using a Gatan model 652 double tilt heating holder for a range of temperature from 35-500 ˚C. Sublimation was observed for template grown Te nanowires with a specific range of diameters from 20-90nm. In-situ video tracks the anisotropic sublimation of the freed individual nanowires in live time with the rate of sublimation observed and compared for different diameter nanowires. Two different sublimation routines are identified and examined: constant sublimation and terrace ledge [3]. The flux of molecules leaving the system can be described by the Hertz-Knudson equation and allow for the calculation of the samples vapor pressure and temperature. These are compared to known information.

[1] D J Hellebusch et al. The Journal of Physical Chemistry Letters 6.4 (2015) 605-611
[1] P Bartlett et al ChemElectroChem 1 (2014) 187-194
[2] C L Hsing et al Anal Chem 87 (2015) 5584-8

P:12 (Flash presentation) Optimising automated quantification of nanoparticle compositions using scanning transmission electron microscope spectrum imaging

Y Wang, T J Slater, P O'Brien and S J Haigh

University of Manchester, UK

Recent developments in scanning transmission electron microscope (STEM) instrumentation have allowed measurement of, the morphology, size and elemental distribution of nanomaterials with sub-nanometer accuracy[1]. However, traditional data analysis relies on time-consuming manual feature identification, or involves presenting only a few images with qualitative descriptions and statistics [2].

The lack of quantitative and automatic analysis of the population, shape specificity, structure details and elemental information of nanomaterials can now be overcome by advanced computational analysis [3]. In this study, AgPt nanoparticles are examined using a FEI field-emission gun Talos STEM, in order to acquire high-angle annular dark-field (HAADF) images and corresponding energy dispersive x-ray (EDX) spectrum image data. A variety of particle detection and segmentation algorithms have been explored and optimised in order to automatically extract size, morphology and compositional data for a large number of individual particles. The surface roughness of each nanoparticle is analysed and is shown to correlate with nanoparticle composition and the synthesis method employed.

The results from this study provide new insights to improve our understanding of the mechanisms of AgPt nanoparticle synthesis. However, more generally we illustrate an automated and flexible approach to extract quantitative information from STEM spectrum image data. The methods developed in this study can be extended to any nanoparticle population, or even precipitates extracted from metallic alloys [4,5].

[1] Haigh, S *Nanosci. Vol 1 Nanostructures through Chem.* 1, 89–101 (2013).
[2] Lewis, E A. *et al. Nanoscale* 6, 13598–13605 (2014).
[3] Laramy, C R. *et al. ACS Nano* 9, 12488–12495 (2015).
[4] Chen, Y Q. *et al. Ultramicroscopy* 144, 1–8 (2014).
[5] Chen, Y Q. *et al. Acta Mater.* 85, 199–206 (2015).

P:13 (Flash presentation) Simulated HAADFSTEM + EDS Tomography of Sub-22 nm FinFETS

R Aveyard and B Rieger

TU Delft, The Netherlands

The next generation of integrated circuits will require nanometer scale components in order to provide increased circuit densities. To successfully manufacture such components with a high yield, a method of defect detection is needed. This defect detection will require structural and chemical characterization of 3- dimensional structures with near atomic resolution. HAADF-STEM offers a suitably high spatial resolution, whilst EDS can provide the requisite chemical information. These two modalities can be simultaneously acquired, and, when recorded in a tomographic framework, can yield fully 3-dimensional structural and chemical reconstructions of the sample.

EDS mapping has traditionally been limited by its poor signal strength, requiring large acquisition times to yield useful results. However, the latest generation of EDS detectors, with increased collection angles, facilitate reduced acquisition times and provide improved chemical sensitivities. This progress in experimental capabilities alongside the fault detection requirements of the semiconductor industry presents a new impetus to develop highly efficient STEM+EDS tomographic acquisition and analysis procedures.
In order to develop such procedures, 'ground truth' tomographic datasets are required for which the specimen is well defined. Unfortunately, it is not possible to generate such datasets by experimental means. These datasets can, however, be computationally simulated.

Here, a new multislice simulation program is reported that is capable of generating both HAADF-STEM and EDS datasets. By following the multislice protocol, this implementation includes dynamic electron scattering effects such as electron channelling, and thus reproduces the realistic non-trivial image formation process that is required to assess the accuracy of tomographic reconstruction techniques.
The new program exploits both multiple CPU cores and multiple GPU cores to minimise calculation times. Using 4 Tesla K40 GPU cards, single image simulations of 5 nm3 subjects can be generated inside 30 minutes.

To provide a 'ground truth' semiconductor dataset, a 25 nm^3 FinFET component model has been produced. This model consists of ~0.5 million atoms of seven different elements with crystalline, amorphous, and poly- crystalline regions, as seen in figure 1. The multislice simulation program has been used to generate HAADF and EDS tomograms of this model, consisting of 179 projections in 2 degree increments. Projections from this tomogram can be seen in figure 2.

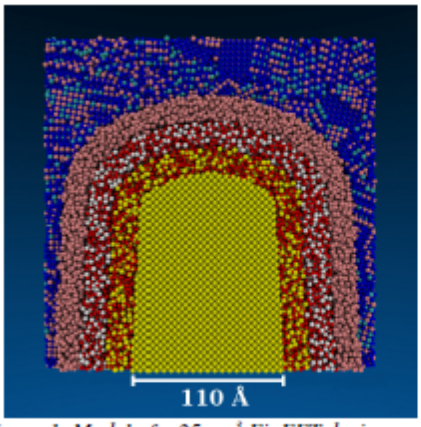

Figure 1. Model of a 25 nm^3 FinFET device

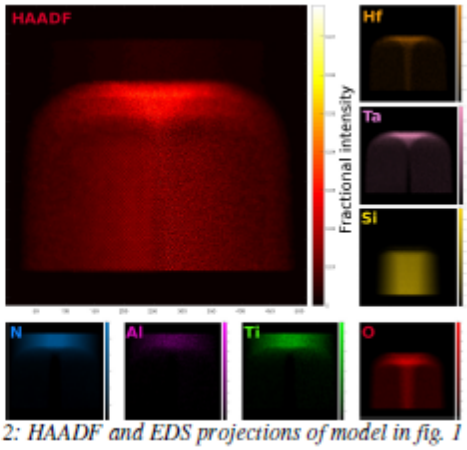

Figure 2: HAADF and EDS projections of model in fig. 1

P:14 (Flash presentation) Quantitative structural and compositional studies of catalyst nanoparticles using annular dark field imaging and spectroscopy

A M Varambhia[1], L Jones[1], D Ozkaya[2], S Lozano-Perez[1] and P D Nellist[1]

[1]University of Oxford, UK, [2]Johnson Matthey Technology Centre, UK

Proton Exchange Membrane Fuel Cells (PEMFC) are one of the most popular and dominant fuel cells present in the market and have the potential to replace fossil fuels in the near future. In order to improve their efficiency the PEMFC field constantly goes through an iterative research and design process. One such research area is catalyst design, where the aim is to focus on improving efficiency of the complex cathode exchange processes within the PEMFC.

There are fundamental considerations to take into account when creating and understanding these catalysts at the nanoscale which still need further investigating. Annular Dark Field Scanning Transmission Electron Microscopy (ADF STEM) provides a useful range of signals (ADF, energy dispersive x-rays (EDX), electron energy loss signals (EELS)) which can be acquired simultaneously to characterise catalyst properties at atomic resolution.

With the introduction of aberration corrected microscopes it is now routinely possible to image catalyst nanoparticles at atomic resolution and gain high resolution analytical information. In the work presented here, some of the most efficient catalysts (Ru, Pt and Pt-Co alloy nanoparticles) reported in literature were imaged and characterised. Using methods recently developed[1-3], such as using scattering cross-sections from the ADF signal to quantify thickness, the catalysts were characterised for size, shape, composition and structure. The formation of stable fcc raft like Ru crystals when the Ru catalyst was exposed to the electron beam are presented. Recent results using a rapid particle size measuring algorithm are presented for Pt and Pt-alloy nanoparticles. Furthermore, three dimensional structure and shape results of Pt nanoparticles are also presented. Finally some EDX and EELS results are discussed to attempt to decouple composition and thickness effects when quantifying alloyed nanoparticles.

[1] H E, K E MacArthur, T J Pennycook, E Okunishi, a J D'Alfonso, N R Lugg, L J Allen, P D Nellist, Ultramicroscopy 2013, 133, 109
[2] K E Macarthur, T J A Slater, S J Haigh, D Ozkaya, P D Nellist, S Lozano-perez, Microscopy and Microanalysis, 2015, In press
[3] L Jones, K E MacArthur, V T Fauske, A T J van Helvoort, P D Nellist, Nano Lett. 2014, 14, 6336

P:15 (Flash presentation) Modal decomposition for 2D and 3D STEM-EELS analyses of surface plasmons in gold and silver nanoparticles

S M Collins[1], E Ringe[2], S J Barrow[1], M Duchamp[3], D Rossouw[4], Z Saghi[1], A Funston[5], P Mulvaney[6], G A Botton[4], R Dunin-Borkowski[3] and P A Midgley[1]

[1]University of Cambridge, UK, [2]Rice University, USA, [3]Forschungszentrum Juelich, Germany, [4]McMaster University, Canada, [5]Monash University, Australia, [6]University of Melbourne, Australia

Gold and silver nanoparticles comprise the building blocks of a variety of nanophotonic technologies making use of their strong light scattering and absorption properties for biological and chemical sensing, solar energy conversion and storage, and nano-scale optics. These optical properties arise from strong localized surface plasmon resonances tuned by the shape, size, and dielectric environment of nanoparticles. Scanning transmission electron microscopy electron energy loss spectroscopy (STEM-EELS) is now an established tool for the qualitative assessment of surface plasmons in gold and silver nanoparticles, largely due to the high spatial resolution offered in STEM-EELS but equally due to the sensitivity of electron beam measurements to a wide variety photonic state symmetries accessible by high energy electron beams. In this presentation, applications of non-negative matrix factorization (NMF) techniques for the decomposition of experimental STEM-EELS into spectral and spatial signatures corresponding to modal resonances will be discussed in conjunction with numerical calculations of

nanoparticle eigenmodes and the corresponding surface charge distributions underlying observed surface plasmon modes. Symmetry assignments of modes in a series of three- and four-particle gold spheroid aggregates and tomographic reconstructions of surface charge eigenmodes in a silver right bipyramid will be presented as cases outlining applications of spectral and modal decomposition approaches for the extraction of quantitative optical properties from STEM-EELS of plasmonic nanoparticles.

P:16 (Flash presentation) Systematic study of background subtraction techniques for EELS

V C Angadi and T Walther

University of Sheffield, UK

Quantification of electron energy-loss spectra by background subtraction is usually done by fitting an inverse power-law (AE-r) function to the pre-edge region. The errors associated with background fit and extrapolation have been discussed by Egerton [1] in terms of so-called h-parameters. More sophisticated methods such as multiple linear least square fits have been implemented in software packages such as Hyperspy [2], EELSMODEL [3] and Digital Micrograph [4]. In background subtraction, there is always a trade-off between systematic and statistical errors in quantification of core-losses. In some cases either due to noise, near edge or extended fine structures in preceding edges, the extrapolated background can cross the spectrum, which leads to large systematic under-estimate of the core-loss intensity. Background subtraction techniques with exponential fitting can be explored more systematically and a new approach on how the quantification can be improved by choosing different functions to fit in pre-edge regions will be discussed. In particular, modelled pre-edge backgrounds can be forced to not cross the spectrum by introducing a linear offset function, thereby minimizing the under-estimate of the core-loss. The precision of EELS quantification with respect to spectrometer entrance aperture has been discussed by Bertoni & Verbeeck [5]. Modelling the background can also be explored more extensively by fitting an inverse power-law or exponential fit to the post-ionisation edge and shifting the background curve fitted downwards to pass though the edge onset. This lead to an overestimate of the core-loss. The best background fit and its reliability can be calculated from the error bars associated with the under and over-estimated intensities.

[1] Egerton, R F (2011). Electron energy-loss spectroscopy in the electron microscope, 3rd Edition, Springer, New York
[2] de la Peña et al (2015). HyperSpy 0.8.1. http://hyperspy.org/
[3] Verbeeck, J. (2015). EELSModel 4.1. http://www.eelsmodel.ua.ac.be/
[4] Gatan. (2015). Gatan Microscopy Suite Software http://www.gatan.com/products/temanalysis/gatan-microscopy-suite-software
[5] Bertoni & Verbeeck (2008). Accuracy and precision in model based EELS quantification Ultramicroscopy, 108(8), 782-790

P:17 (Flash presentation) The effect of prior deformation on the phase evolution and phosphorus segregation within an AISI Type 316 austenitic stainless steels

A D Warren, A I Martinez-Ubeda, I J Griffiths and P E J Flewitt

University of Bristol, UK

The effect of prior deformation on the long term thermally induced phase evolution of Type 316austenitic stainless steels is considered for two components with similar compositions manufactured by the same company: one component is a thin walled pipe, which experienced significant working during manufacture, whilst the other, a thick walled boiler header, experienced less. The microstructure of the latter shows distinct regions enriched in chromium and molybdenum, originating from the dendritic structure of the original casting. In addition to compositional differences, these heterogeneous regions have a significantly smaller grain size than the bulk material. The thin walled pipe specimens have a uniform microstructure and elemental distribution due to the fabrication disrupting the dendritic structure. Following prolonged ageing at ~500 °C both components evolved different ranges of secondary phase precipitates, despite their similar composition. Precipitate identification was achieved with high resolution (S)TEM imaging and composition microanalysis, undertaken using a JEOL ARM instrument operating at 200 keV. The Cr and Mo enriched regions in the boiler header showed a complex mix of precipitates including (high Fe) α-ferrite, δ-ferrite, $M_{23}C_6$ carbide, Chi-phase, G-phase and γ' after ~87,000 hours. The thin walled pipes showed $M_{23}C_6$ carbide, δ-ferrite and G-phase after ~160,000 hours ageing, which was similar to the bulk regions of the boiler header. Detailed microanalysis revealed that for the boiler header material P segregates to the chi-austenite phase boundaries, whilst in the more uniform thin walled pipes P segregates to the $M_{23}C_6$-austenite phase boundaries. The reasons for these differences in behaviour and distribution are discussed, along with the implications for fracture and creep deformation characteristics of these materials.

P:18 How does the carbon source affect carbon nanotube chirality in floating catalyst CVD?

J S Barnard, C Paukner and K K K Koziol

University of Cambridge, UK

Floating catalyst chemical vapour deposition (CVD) is a technqiue for producing large quantities of carbon nanotubes (CNTs) continuously. We have studied how the molecular source of carbon, i.e. the precursor molecule, that is pyrolized in a continuous-flow reactor, affects the CNT chirality that emerges from the exhaust. Electron diffraction of large populations of CNTs (> 60 tubes) show that substantial changes occur to both the CNT type, i.e. single-wall or double-wall CNTs (DWNTs), the diameter distribution and the inter-wall distance in DWNTs. We find that ethanol and toluene behave similarly, i.e. they produce about 90% SWNTs with narrow diameter ranges (1.1 to 1.7nm for ethanol, 1.3 to 2.3nm for toluene), with the ~10% DWNTs showing chiral correlations between inner and outer walls with a tight spacing (0.29nm). Methane produces larger DWNTs (1.2 to 4.6nm inner; 2.2 to 5.3nm outer) with weak chiral correlations and large inter-wall spacings (0.39nm). The CNT chiralities follow the trends predicted by our current understanding of growth models, but the inter-wall spacing variation remains poorly understood. We will discuss several mechanisms that might explain this.

P:19 Electron nanofocusing using perforated nanoparticles

Z Cao and G Möebus

University of Sheffield, UK

Non-standard, i.e. non-electromagnetic, methods of focusing charged particle beams are mainly known from focused ion beam instruments, but also used in research on parallel electron lithography, and for miniature electron microscope designs consisting of sequences of electrostatic apertures using micro-fabrication [1]. Another extreme proposal was the "atomic focuser" aiming at 0.05nm resolution HRTEM. [2] Surprisingly little evidence is available for focusing with 1-10nm sized holes, fitting in between the above approaches which are either on micro-level or atomic-level, although HRTEM of holes in crystals have been simulated for materials science purpose [3]. Using JEMS image simulations, the formation of focused spots is examined for various model objects, including: (i) supercells with central array of columns removed, (ii) nanoparticles with central holes, (iii) artificially amorphized supercells to suppress any channeling, and (iv) focusing by partially drilled holes using a mixture of full and perforated supercells. The main parameters, image focus, thickness and envelope functions, are tuned to achieve suppression of lattice fringe visibility (opposite to the aims in materials science), while maximising the formation of a small and bright central focus spot, which in intensity should be well exceeding any trivial "shadow formation" of a projected hole, and in fact be much smaller than the hole. Computational results for two atomic number materials are used and preliminary comparison to experimentally perforated nanoparticles is presented. Apart from relevance for lithography-related applications, the simulations are also meant to help to understand image details upon (non-intentional) formation of holes and partially drilled holes during chemical spot analysis.

[1] B J Kampherbeek, M J Wieland, and P Kruit, J Vac Sc Tech B 18 (2000) 117
[2] J M Cowley, J C H Spence, Valery V. Smirnov, Ultramicroscopy 68 (1997) 135-148
[3] K Scheerschmidt, R Hillebrand, Ultramicroscopy 33 (1990) 27-39

P:20 Electron beam writing in oxide glasses via irradiation induced metal nanodots

M M Sabri and G Möebus

University of Sheffield, UK

Oxide glasses are well known substrates and targets for irradiation induced generation of spatially localised metal nanoparticle patterns. Mostly achieved by laser-irradiation (and occasionally by ion or gamma irradiation) through photo-reduction of glassdopant species, there is relatively little research about the electro-beam nanoscale equivalent method. We have used thermionic and field-emission TEMs at 200 and 300 kV to locally irradiate borosilicate (BS) glass fragments with large variation of target metal concentration: (i) a Zn-BS glass (60mol% ZnO) for Zn-metal patterning represents a type of glass where the precipitate comes from a majority constituent; (ii) a Cu loaded BS-glass (20mol% CuO) represents an example with medium concentration of the target metal species; and (iii) an Ag loaded cerium-borosilicate glass with only 1-2mol% Ag_2O represents a glass with small dopant contribution, where the extra Ce doping offers the opportunity to study Ag-Ce redox interaction during precipitation. The experiments are aiming at illustrating future capabilities of glass surface (and refractive index) engineering with respect to reflectivity, wave guiding, nano-plasmonic light coupling, and potentially catalysis, as promising application fields, apart from also revealing insight into multi-component glass behaviour under irradiation relevant to nuclear waste immobilisation.

As a result, in all three glass groups it was possible to form metallic nanoprecipitates under the electron beam at pre-selected positions, however, with varying quality of patterns. Challenges include (i) speed of precipitation (high enough to get high particle densities in line-scans, and low enough to prevent pre-forming during image focusing), (ii) de-localisation, i.e. avoidance of particles forming mainly on the outside of the beam, leading to double-lines and circle-patterns, (iii) fabrication of metal particles in the inside rather than on the glass surfaces, and (iv) avoiding of excessive glass matrix ablation (glass thinning) during patterning.

The influence of microscope parameters (irradiation dose with and without condenser-aperture inserted), beam resolution, ion migration inside the glass, and specimen geometry parameters on the blurring and quality of spot and line-writing attempts are presented, and particle identities are derived mainly from EELS assisted by HRTEM and EDX.

P:21 Dynamical and thermal properties of the rock salt MgS and MgSe compounds

Y Chaouche and B M Loutfi

Université Larbi Tebessi, Algeria

We present in this work the calculated of the structural, elastic, lattice dynamical and thermal properties of the rock salt (B1) MgS and MgSe compounds using the plane wave and pseudopotentials method (PP-PW) in the frame work of the density functional theory DFT within Local Density Approximation LDA. The structural parameters such as lattice constant and bulk modulus are calculated by minimizing the energy with respect to volume and compared very well with experimental and other theoretical data. The density Functional Perturbation Theory (DFPT) is applied to determine the phonon dispersion relations along the high symmetry lines; all phonon modes have positive frequencies indicating the stability of these compounds in this structure. Using the calculated phonon density of states, the thermodynamic functions of the rock salt MgS and MgSe compounds are determined such as entropy, heat capacity, internal energy and Helmholtz free energy.

P:22 Elongated silicon–carbon bonds at graphene edges

Q Chen[1], A W Robertson[1], K He[1], C Gong[1], E Yoon[2], A I Kirkland[1], G-D Lee[2] and J H Warner[1]

University of Oxford, UK, Seoul National University, South Korea

Dopants in graphene, including nitrogen, silicon (Si) and iron, are able to significantly alter the electronic properties of the host material, even at extremely low doping levels of one dopant per hundred million carbon atoms.1,2 They can also play important roles in catalysis, especially N doped graphene. We study the bond lengths of Si atoms attached to both armchair and zigzag edges using aberration corrected transmission electron microscopy (AC-TEM) with monochromation of the electron beam.3 An in situ heating holder is used to perform imaging of samples at 800 °C in order to reduce chemical etching effects that cause rapid structure changes of graphene edges at room temperature under the electron beam. We provide detailed bond length measurements for Si atoms both attached to edges and also as near edge substitutional dopants. Edge reconstruction is also involved with the addition of Si dopants. Si atoms bonded to the edge of graphene are compared to substitutional dopants in the bulk lattice and reveal reduced out-ofplane distortion and bond elongation. An extended linear array of Si atoms at the edge is found to be energy-favourable due to inter-Si interactions. These results provide detailed structural information about the Si–C bonds in graphene, which may have importance in future catalytic and electronic applications.

P:23 Understanding the epitaxial growth mechanisms of metal oxide nanoislands on strontium titanate substrates via transmission electron microscopy

X Cheng[1], J Sullaphen[1], M Weyland[2], H Liu[3], J Liu[1] and N Valanoor[1]

[1]University New South Wales, Australia, [2]Monash University, Australia, [3]University of Sydney, Australia

The strong and aggressive push for higher density and faster performance has pushed the size of multifunctional devices into the nanoscale regime. Irrespective of the ultimate functionality, the nanoscale functional material has to be integrated on to a substrate to make a viable and robust device. In oxide nanoelectronics, often these functional devices are realized via heteroepitaxial growth of the nanoislands or thin films on a selected oxide substrate. Thus understanding the growth mechanism of the metal oxide nanoislands on selected substrates and being able to predict their possible morphologies are critical in order to fabricate high quality nanoscaled functional devices.

Here we show two cases of our studies in understanding the heteroepitaxial growth mechanisms of metal oxide nanoislands grown on strontium titanite ($SrTiO_3$: STO) substrates: the strain and chemical driven substrate deformation of nickel oxide (NiO) single crystal nanoislands grown on STO substrate; and the multiple orientation relationships between manganese oxide (Mn_3O_4) nanoislands and STO substrate via invariant deformation element (IDE) model.

For the first case, aberration corrected high angle annular dark field scanning transmission electron microscope (HAADF-STEM) and high-resolution bright field TEM reveal that the substrate is heavily deformed due to the influence of the interfaces created by an epitaxial NiO nanoisland. The substrate is deformed so as to back-fill around the bottom facets of the NiO nanoislands and form a caldera structure in order to promote wetting. Furthermore it is likely that the redox reaction at the island-substrate interface contributes to the distortion of the interfaces.

In the second case study we use an IDE model to successfully predict the orientation relationships and interfaces between Mn3O4 nanoislands grown on STO substrate for three principle cubic surface planes, namely $(001)_{STO}$, $(110)_{STO}$ and $(111)_{STO}$. It reveals that the diversity of growth orientation could be rationally interpreted by the nature of invariant strain line and twinning relationships of deposited materials. We show how this model can also be applied to the prediction of crystallographic orientation relationships in other epitaxial growth systems.

P:24 Determining optimum sample thickness for TKD using AZtec

K Dicks[1], J Goulden[1] P Trimby[2], S Piazolo[3], Z Chen[2] and G Sneddon[2]

[1]Oxford Instruments, UK, [2]University of Sydney, Australia, [3]Macquarie University, Australia

Since its development, the application of Transmission Kikuchi Diffraction (TKD) in the scanning electron microscope (SEM) has become an increasingly frequently used technique for the nanostructural characterisation of materials [1-3].

The TKD technique, involves a standard EBSD system fitted to a field emission gun (FEG) SEM, and achieves spatial resolutions on the scale of 2-10 nm. This has enabled researchers to carry out orientation mapping on samples with grain sizes significantly below 50 nm, something that would have been impossible using conventional EBSD.

The key to the improved spatial resolution of TKD is the use of electron transparent samples, such as those prepared for standard transmission electron microscopy (TEM). In, most commercial SEMs however, the beam energies are limited to 30 kV, and so there is significantly more electron scattering through the sample thickness when analysing using TKD with respect to TEM. This means that the sample thickness is critical: too thick and the electron beam will scatter more broadly and there will be a significant loss of resolution, too thin and there will be insufficient diffracted signal to enable effective and fast measurement. In addition, the preparing of electron transparent samples using a focused ion beam (FIB) SEM can result in amorphisation of the sample surface due to Ga ion implantation. As the

dominant signal for TKD comes from the lower surface of the sample, Ga-damage can cause complete loss of the diffraction pattern and prevent successful analyses.

This poster describes a method of determining and quantifying both of these challenges; both the optimum sample thickness for TKD and the level of Ga implantation in TEM foils.

[1] R R Keller and R H Geiss, J. Microscopy 245 (2012), 245-251
[2] P W Trimby, Ultramicroscopy 120 (2012), 16-24
[3] P W Trimby et. al., Acta Materialia, 62 (2014), 69-80

P:25 Chemical and structure analysis of soft and bio-materials

M Falke[1], A Kaeppel[1], R Terborg[1], T Salge[2], C Slomianny[3], N Musat[4], S Boehm[1], J Berlin[5] and D Goran[1]

[1]Bruker, Germany, [2]Natural History Museum London, UK, [3]Lille University, France, [4]Helmholtz Centre for Environmental Research, Germany, [5]EDS and WDS Coaching, Germany

Chemical and structure characterization is essential for understanding the function of soft and biological materials and for respective new approaches in life science, medicine, nano-toxicity and the development of bio-inspired devices. Using various examples, this contribution demonstrates available analysis instrumentation for chemical and structural characterization from the mm to the atomic scale.

Energy dispersive X-ray spectroscopy (EDS) in electron microscopy (SEM/TEM) allows mapping the element distribution of light (N, C, O) and heavy elements (Ag, Pt, U) with high efficiency. Multiple detector arrangements ensure a large collection angle and overcome shadowing effects. Samples can be investigated fast and in a close to natural state. Some of the examples of SEM-EDS studies are the embedding of skin irritating calcium oxalate crystals into the agave leaf, the distribution of nano-clay in a highly topographic polymer sample and the element distribution in insects. Examples exploring the capabilities of STEM-EDS are the quantitative investigation of the iron intake of a malaria parasite in a human blood cell and of the light element distribution in this cell and the visualization of different metal containing protein labels used in cell biology. EDS in combination with aberration corrected STEM allows monitoring light and heavy elements on the atomic level [1].

An exemplary electron backscatter diffraction (EBSD) study of birds egg shells reveals why a stable egg shell is easy to crack from the inside. Similar analysis approaches can be used for the characterization of apatite related structures such as shells, teeth, bone, bone templates etc.

Non-destructive 3D analysis by X-ray micro-tomography was used to understand structures for heat protection on the small scale [2]. A micro-CT attachment for SEM allows to further increase spatial resolution of this 3D analysis technique to half a micrometer.

X-ray fluorescence analysis allows mapping of trace elements on a larger scale and in deeper sample levels than possible using EDS.

[1] Lovejoy T C et al., Appl. Phys. Lett. 100 (2012) 154101; R. M. Stroud et al., Proceedings M&M (2015)
[2] Verdú, J R, et al., M. PLoS ONE: 7(3): 1-9, (2012)

P:26 Thermally induced dynamics of dislocations in graphene at atomic resolution

C Gong[1], A W Robertson[1], K He[1], G-D Lee[2], E Yoon[2], C S Allen[1], A I Kirkland[1] and J H Warner[1]

[1]University of Oxford, UK, [2]Seoul National University, Korea

The exceptional properties of graphene can be modulated by introducing defects and dislocations into the lattice. The movement of dislocations also plays a crucial role in determining the macroscopic plastic deformation of materials, especially at elevated temperatures. In this report we use an in situ heating holder in an aberration corrected transmission electron microscopy to study the movement of dislocations in suspended monolayer graphene up to 800 °C. Control of temperature enables the differentiation of electron beam induced effects and thermally driven processes. At room temperature, the dynamics of dislocation behaviour is driven by the electron beam irradiation at 80 kV; however at higher temperatures, increased movement of the dislocation is observed and provides evidence for the influence of thermal energy to the system. An analysis of the dislocation movement shows both climb and glide processes, including new complex pathways for migration and large nanoscale rapid jumps between fixed positions in the lattice. The improved understanding of the high temperature dislocation movement provides insights into annealing processes in graphene and the behaviour of defects with increased heat.

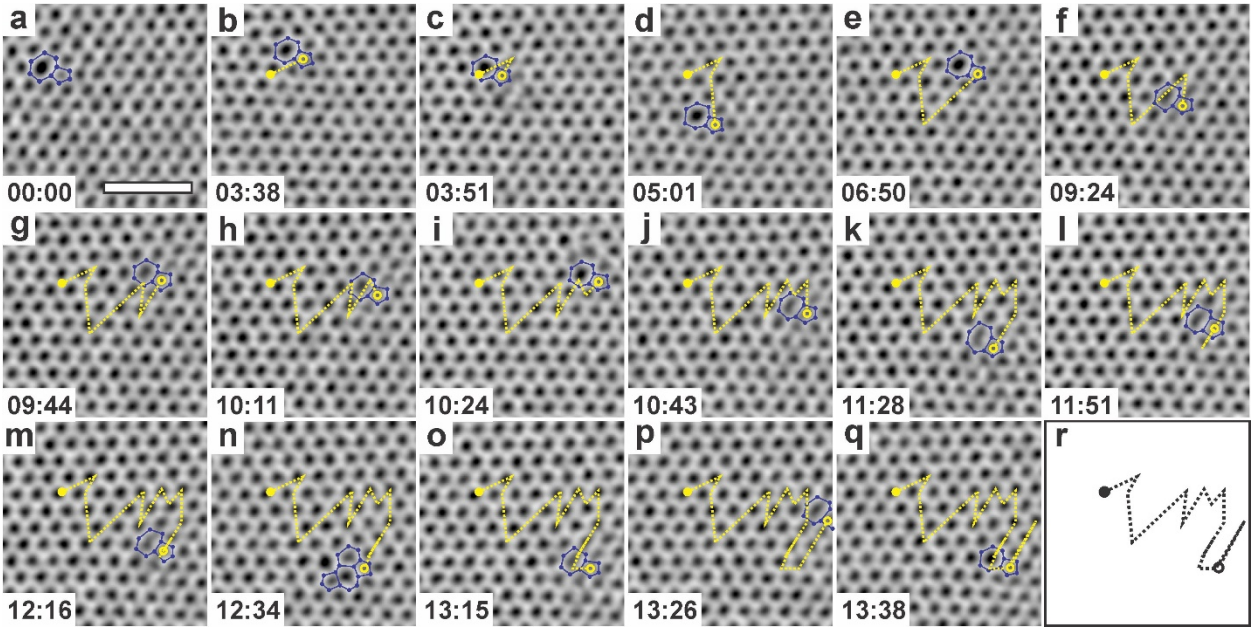

[1] Gong, C et al, ACS Nano, 9 (2015) p. 10066–10075
[2] Warner, J H et al, Science 337 (2012) p. 209–212

P:27 Aberration corrected electron energy loss spectroscopy analysis of irradiated UO_2 epitaxial films.

I Griffiths, S Rennie, J E Darnbrough, T B Scott and R Springell

University of Bristol, UK

A key limitation of using Uranium Dioxide as a nuclear fuel is the significant effect of irradiation damage on the crystal structure. The changes undergone are not fully understood at a microscopic level, with most research being performed on bulk material. In order to investigate the effect of irradiation on UO_2, an epitaxial thin film grown via Reactive DC Magnetron Sputtering, has been irradiated with 2.1 MeV He^{2+} ions to achieve a damage of 0.15 dpa, simulating the damage induced during reactor operation. Following the irradiation, the sample has been studied using a JEOL ARM 200F aberration corrected STEM operating at 200kV and analysed using Electron Energy Loss Spectroscopy (EELS) to determine the nature of defects found. Comparison of the irradiated material with a pristine film grown under identical conditions have revealed the presence of small features measuring ~ 8 nm in diameter. The exact nature of these features is not yet fully understood but EELS analysis has suggested a presence of either voids or He bubbles within the material. The presence of these features could lead to changes in the material properties such as a reduction in thermal conductivity, limiting the efficiency of UO_2 as a nuclear fuel.

P:28 On the HREM contrast from 0001 planes in wurtzite GaAs

C Hetherington

Lund University, Sweden

HREM images taken down the 1,1,-2,0 zone axes of wurtzite crystals often display periodicities that correspond to the d(0001) interlayer spacing, even though 0001 is a kinematically forbidden reflection. This 1, 1, -2 0 orientation is regularly used in the characterisation of nanowires to differentiate areas of wurtzite structure having ABAB stacking and areas of zinc blende structure having ABCABC stacking. In order to be more secure about the characterisation, a study has been made of this unexpected contrast. Essentially, it can be explained by a tilt of the crystal away from the exact zone axis orientation relative to the incident beam, with the specimen thickness also playing a role.

This study built on the work of Bow et al (1996) who looked at the crystallographic origin of the alternate bright/dark contrast in 6H-SiC and other hexagonal crystal HREM images. GaAs in its wurtzite form (found regularly in nanowires) is hexagonal, as is the effective supercell of multiple twin bands in zincblende GaAs and the effect is seen in each case. Experimental observations were made both of HREM imaging and convergent beam diffraction and compared to simulations, for GaAs and GaN. Thus we ccould make a quantitative appraisal of the magnitude of the contrast for different tilts and thicknesses and estimate how accurately one needs to align the crystal to avoid the effect.

[1] Bow, J S, Carpenter, R W, & Kim, M J (1996). *Microscopy and Microanalysis*, *2*(02), 63-78

P:29 Accurate EPMA quantification of the first series transition metals using LI lines

I Holton [1], C Hombourger [2] and M Outrequin[2]

[1]Acutance Scientific Ltd, UK, [2]CAMECA, France

In conventional EPMA, X-ray K lines are used for accurate quantification of the transition metal elements. However, at low beam accelerating voltages (i.e., < 5 keV), only low-energy X-ray lines are emitted, including K lines for Z ≤ 22 and L and M lines for Z > 22. Low beam energy operation offers several advantages: improvement of analytical spatial resolution and reduction of both secondary fluorescence and sample charging effects. The use of low-energy X-ray lines for quantitative analysis does present new analytical challenges, though, because these lines are subject to larger peak shifts, more line overlaps and lower fluorescence yields, as compared to higher-energy K lines. The low yields also reduce the intensity of certain lines, as does the low overvoltage, U (defined as the ratio of beam energy to ionization energy for a given line), which lowers the ionization probability for the X-ray line.

If we consider the example of Fe (Z=26) analyzed at 15 keV, many characteristic X-ray lines (K- and L-series) are produced from the atom. The X-ray lines traditionally used for quantification are the K□ line (transition from L_3 sub-shell to K sub-shell) and L□ line (transition from M_5 sub-shell to L_3 sub-shell). Generation of the Fe L□ line involves valence electrons, which are affected by the chemical bonding of Fe in the target sample. Wavelength shifts, peak shape modifications, and increases or decreases in the relative intensities of the characteristic lines can be readily observed between different chemical types.

In general, for elements of the first transition metal series (Sc to Zn), the pattern of L emission spectra varies according to the energy of the incident electrons (E_0), as follows:

- E_0 between the L_3 and L_2 threshold energies: intensity of the high energy satellite lines is reduced.
- E_0 from the L_3 sub-shell threshold energy up to 3 times this energy: excitation and development of the high energy satellites increases and the shape of the L □ line becomes increasingly distorted
- E_0 above 3 and 4 times the L_3 sub-shell threshold energy: the absorption path of the generated X-rays increases and thus the fine structure on the high energy side “disappears” due to self-absorption.

From these spectroscopic observations, it becomes obvious that the shape and the peak position of the L emission band is strongly dependent on the incident electron energy and thus can lead to inaccuracies in quantification when using L□ lines.

As an alternative, Fialin et al. [1] have suggested the use of the Ll line, instead of the more commonly used Lα or Lβ lines. The Ll line has the advantage of being independent of the chemical state of the element, since the electrons of the outer shell involved in the Ll transition are core, not valence, electrons. One drawback is the low intensity of Ll, compared to the Lα line (typically 10 times less for Fe measured with a TAP crystal). Quantitative results achieved by using the Ll lines for the elements of the first transition series will be presented.

Figure 2: Energy level diagram showing electron transitions producing Fe K and L X-rays.

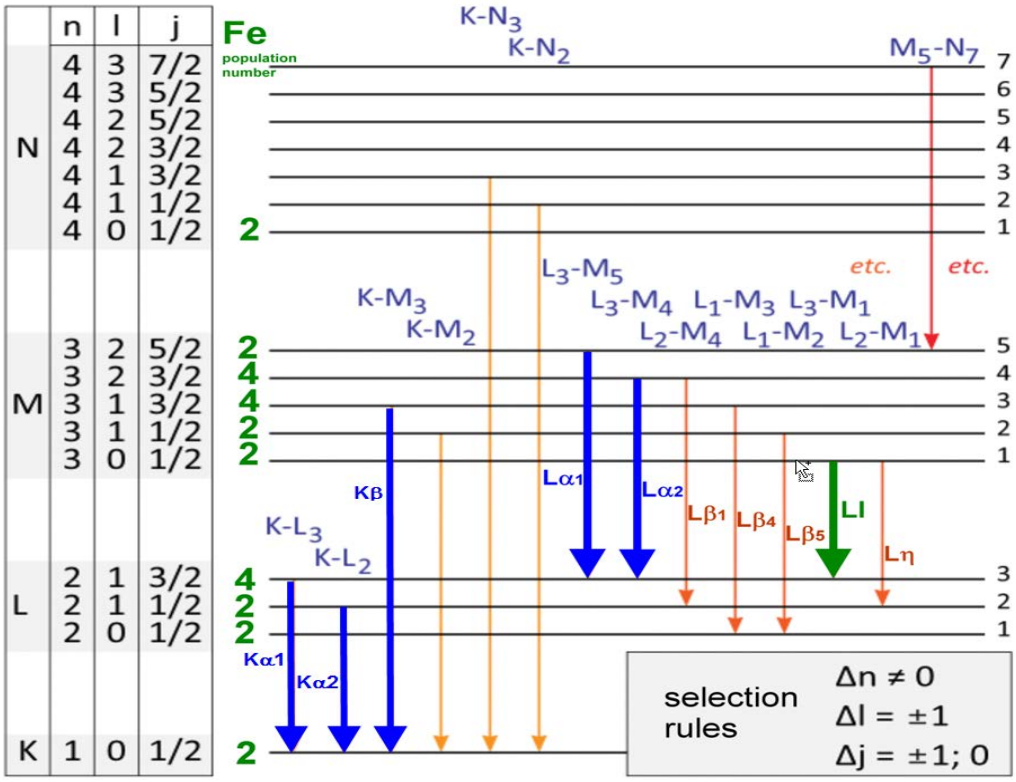

[1] Fialin M, Wagner C and Remond G, 1998 in: Proceedings, EMAS'98, 3rd Regional Workshop.

P:30 Evaluating the electron beam sensitivity of calcium carbonate based materials

R W M Hooley[1,2], R M Drummond-Brydson[2] , A P Brown[2] and F C Meldrum[2]

[1]EPSRC Centre for Doctoral Training in Complex Particulate Products and Processes (CDT-CP3), UK, [2]University of Leeds, UK

Calcium carbonate is a common material, most often encountered as biominerals such as seashells or in the environment. It appears as three crystalline anhydrous polymorphs, but related amorphous or poorly crystalline forms are also known. Calcium carbonate is of widespread interest as both a structural biomaterial and for its environmental and industrial importance, which has led to extensive research into its formation and properties. Transmission electron microscopy (TEM) can be used to probe the structures and compositions of a variety of calcium carbonate based systems, allowing for a greater understanding of their formation and function. Whilst a heavily researched material, calcium carbonate is well known for its sensitivity under electron irradiation [1-3], limiting the amount of analytical information that can be extracted without damaging the region of interest. This is especially the case with biological forms which often occlude proteins. This appears to increase the materials sensitivity to electron irradiation. This research investigates quantitatively the irradiation-induced damage of calcium carbonate polymorphs, nanostructures and composites, with the goal of extracting electron flux and total electron fluence conditions where repeatable imaging and analytical (both scanning TEM and conventional TEM) data can be extracted without sample damage.[4] By understanding the irradiation induced degradation of calcium carbonate, it will be possible to develop damage limitation strategies which can also be applied to other sensitive systems.[5]

[1] Kim Y-Y, Schenk A S, Ihli J, Kulak A N, Hetherington N B J, Tang C C, Schmahl W W, Griesshaber E, Hyett G and Meldrum F C 2014 A critical analysis of calcium carbonate mesocrystals Nat Commun 5

[2] Hoffmann R, Wochnik A S, Betzler S B, Matich S, Griesshaber E, Schmahl W W and Scheu C 2014 TEM preparation methods and influence of radiation damage on the beam sensitive CaCO3 shell of Emiliania huxleyi Micron 62 28-36
[3] Kabalah-Amitai L, Mayzel B, Kauffmann Y, Fitch A N, Bloch L, Gilbert P U P A and Pokroy B 2013 Vaterite Crystals Contain Two Interspersed Crystal Structures Science 340 454-7
[4] Egerton R F, Li P and Malac M 2004 Radiation damage in the TEM and SEM Micron 35 399-409
[5] Egerton R F 2013 Control of radiation damage in the TEM Ultramicroscopy 127 100-8

P:31 Structure study of mesoporous silica templates by phase restoration of focal series of images

R J Kashtiban[1], A Lodge[2], A L Hector[2], G Reid[2], P N Bartlett[2], J Sloan[1], D C Smith[2] and R Beanland[1]

[1]University of Warwick, UK, [2]University of Southampton, UK

Determining the structure of porous materials with extended structure is vital for understanding and adapting their function. Transmission electron microscopy (TEM) is widely used to achieve this, but due to the weak electron scattering cross-section of this materials with extended structure and high surface to volume ratio, TEM images of these category of technologically important materials are generally low contrast and low resolution. Exit wave reconstruction (EWR) of focal series of TEM images has previously applied successfully on the study highly ordered carbon based materials in atomic scale with sub-angstrom resolution [1]. Here we present a routine to achieve high-contrast imaging of mesoporous silica using EWR, revealing a new level of structural detail. We apply EWR on mesoporous silica templates to study structure and more importantly accurate metrology of the diameter of the pores with rough internal surface distinguishing not only the general morphology or nanostructure and their accessibility but also accurate measurement of the pore size. This accurate pore size evaluation is important factor in functionality of these materials as a template for growth of highly ordered nanowire on substrates such as silicon for device applications.

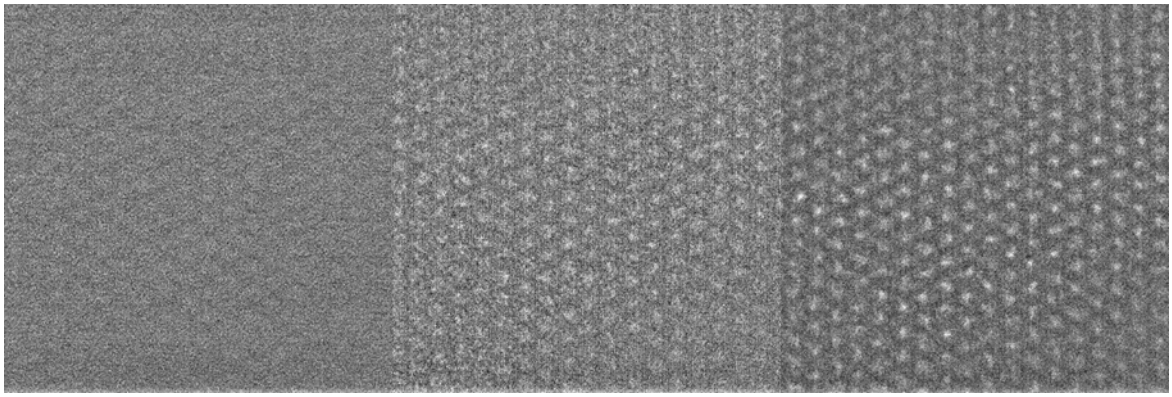

Figure 1. Effect of defocus on the contrast of TEM-BF images of a mesoporous silica film at (left) 100 nm focus, (middle) -200 nm focus and (right) -300 nm defocus.

[1] R J Kashtiban, A Dyson, Rahul Nair, R. Zan, J Sloan, U Bangert and A. *Geim,*" Atomically Resolved Imaging of Highly Ordered Alternating Fluorinated Graphene" Nature Comm., 5 (2014) 4902

P:32 Insight into the physical chemistry of Nanoalloys from aberration-corrected HAADF- STEM

Z Li

Nanoscale Physics Research Laboratory, UK

Nanoalloys are alloyed nanoparticles which exhibit tremendous potential in applications from catalysis to nanoplasmonics and data storage, with greater opportunities for tailoring properties than it is possible for their monometallic counterparts. This is because of the synergy between their constituent elements in addition to size and shape effects. To understand the properties of such nanomaterials, a study of the relationship between the structure and chemistry at atomic scale is essential. In this regard, aberration-corrected highangle annular dark field scanning transmission electron microscopy (HAADF-STEM) plays an important and indispensable role. Here, through examples of a wide range of bimetallic nanostructured systems we have studied using a JEM-2100F 200kV STEM fitted with a CEOS probe corrector in Birmingham, I will highlight the current challenges we face and discuss the need in instrumental developments to further open up exciting opportunities to gain insight into physical chemistry of this unique type of nanomaterials. In support of this, following case studies will be presented: (1) Thermal induced structural transform of AuPd nanoparticles prepared by chemical vapor deposition; (2) Metal-metal bonding in Au-M nanorods (M=Pd, Rh, Pt) synthesized via wet chemical method; (3) Interfacial structures of core-shell CuAg nanoparticles formed by sequential deposition via laser ablation; (4) The role of support on chemistry and stability of AuRh nanoparticles on TiO_2 nanorods; (5) Surface atoms of dendritic Pt_xCu tripods in understanding of enhanced electro-catalytic activity.

P:33 Atomic structure of 1.8 nm monolayer-protected Au_N clusters by aberration-corrected STEM

J Liu, N Jian, A J Pattison and R E Palmer

University of Birmingham, UK

Knowing the atomic structure of monolayer-protected (MP) Au_N clusters is essential to a full understanding of the origin of their intriguing physical and chemical properties. Here we employed aberration-corrected scanning transmission electron microscopy (ac-STEM), combined with multislice simulations to investigate the atomic structure of clusters of core diameter ~1.8 nm, including the nominal composition $Au_{144}(SCH_2CH_2Ph)_{60}$. The MP Au_N clusters were "weighed" against size-selected clusters by the atom counting method [2, 3] and "fractionated" accordingly. The mean nuclearity of the MP Au_N clusters was 122 ± 9. We used Au cluster models of several different sizes for atomic structure analysis. In the fraction of clusters containing 144 ± 7 Au atoms, we found that about 11% of these clusters matched the theoretically predicted $Au_{144}(SR)_{60}$ structure [4], while a large proportion of the clusters were amorphous or unidentified. A few clusters were also found to match the $Au_{130}(SR)_{50}$ structure in the smaller size range. Across the whole nominal size range from N=107 to 151 Au atoms, we found a further ~33% of the clusters exhibit a ring-dot motif, characteristic of local icosahedral symmetry.

[1] Liu, J; Jian, N; Pattison, A J; Palmer, R E Atomic Structure of 1.8 nm Monolayer-Protected Au_N Clusters by Aberration-Corrected STEM, submitted
[2] Wang, ZW; Toikkanen, O; Yin, F; Li, Z Y; Quinn, B M; Palmer, R E J Am. Chem. Soc. 2010, 132, 2854–2855
[3] Jian, N; Stapelfeldt, C; Hu, K-J; Fröba, M; Palmer, R E Nanoscale 2015, 7, 885–888
[4] Lopez-acevedo, O; Akola, J; Whetten, R L; Grönbeck H; Häkkinen H. J. Phys. Chem. C 2009, 144, 5035–5038

P:34 Generation of clusters in reflection mode from the Matrix Assembly Cluster Source (MACS)

J Liu[1], F Yin[1,2], W D Terry[1] and R E Palmer[1]

[1]University of Birmingham, UK, [2]School of Shaanxi Normal University, China

Nanoclusters are attracting great attention due to their wide applications and size-dependent properties [1, 2]. But the applications of size-selected nanoclusters are limited by the beam flux [3, 4]. Here we report the production of nanoclusters in the Matrix Assembly Cluster Source (MACS), which has the potential to be scaled up extensively. In this method, vaporized metal atoms and inert gas atoms are co-condensed on a (copper) substrate to form the matrix at low temperature (<20K, cooled by liquid helium). Then a high energy Ar^+ ion beam is used to sputter the matrix at a specific incident angle. In this particular way, the clusters are collected in reflection mode and the substrate is a solid surface.

The clusters produced in the MACS in reflection mode were characterized by aberration-corrected scanning transmission electron microscopy (STEM) in high angular annular dark field (HAADF) mode. The results showed that the Ag cluster flux and size distribution varied with ion beam incident angle, sputtering energy and metal concentration in the matrix. The cluster flux was found to be maximised for an incident angle of 10° with respect to the surface. The optimal reflection angle changed with the incident angle, but the angle between them was almost constant, close to 110°. The cluster size distribution did not change much with incident angle, but depended on the sputtering energy and metal concentration.

[1] S Palomba and R E Palmer, Optical coupling of core-shell quantum dots to size-selected gold clusters, J. Appl. Phys. 104, 094316 (2008)

[2] F Yin, S Lee, A Abdela, S Vajda and R E Palmer. Communication: Suppression of sintering of size-selected Pd clusters under realistic reaction conditions for catalysis, J. Chem. Phys. 134, 141101 (2011)

[3] C H Zhang, H Tsunoyama, H Akatsuka, H Sekiya, T Nagase, A Nakajima. Development of cluster ion source based on modulated pulse power magnetron sputtering technique, Nano/Micro Engineered and Molecular Systems (NEMS), 8th IEEE International Conference, 428-431 (2013)

[4] S Pratontep, S J Carroll, C Xirouchaki, M Streun and R E Palmer, Size-selected cluster beam source based on radio frequency magnetron plasma sputtering and gas condensation, Rev. Sci. Instrum. 76, 045103 (2005)

P:35 Pt Diffusion dynamics on the formation Cr-Pt core-shell nanoparticles

G Gupta[1], P Iqbal[1], F Yin[1,2], J Liu[1], R E Palmer[1], S Sharma[1], K C-F Leung[3] and P M Mendes[1]

[1]University of Birmingham, UK, [2]Shaanxi Normal University, China, [3]The Hong Kong Baptist University, Hong Kong SAR.

Bimetallic nanoparticles are of wide interest due to the possibility to enhance or attain novel properties that cannot be reached in nanoparticles from pure metals. Layered core-shell bimetallic Cr-Pt nanoparticles were prepared by the formation and later reduction of an intermediate Pt ion-containing supramolecular complex onto pre-formed Cr nanoparticles. The resultant nanoparticles were characterised by X-Ray diffraction analysis, transmission electron microscopy, X-ray photoelectron spectroscopy and aberration-corrected scanning transmission electron microscopy. The results are consistent with the presence of Pt diffusion during or after bimetallic nanoparticle formation, which has resulted in a Pt/Cr-alloyed core and shell. We postulate that such Pt diffusion occurs by an electric field-assisted process according to Cabrera-Mott theory, and that it originates from the low work function of the pre-formed oxygen defective Cr nanoparticles and the rather large electron affinity of Pt.

[1] G Gupta, P Iqbal, F. Yin et al. Pt Diffusion Dynamics on the Formation Cr-Pt Core-Shell Nanoparticles, *Langmuir*, 2015, 31, 6917–6923

P:36 Transition radiation artefacts in TEM-CL imaging and spectroscopy

B Mendis[1], A Howkins[2], D Stowe[3], J Major[4] and K Durose[4]

[1]University of Durham, UK, [2]Brunel University, UK, [3]Gatan UK, UK, [4]University of Liverpool, UK

There is renewed interest in cathodoluminescence (CL) in the transmission electron microscope, since it can be combined with low energy loss spectroscopy measurements and can also be used to probe defects, such as grain boundaries and dislocations, at high spatial resolution. Transition radiation (TR), which is emitted when the incident electron crosses the vacuum-specimen interface, is however an important artefact that has received very little attention. The importance of TR is demonstrated on a wedge shaped CdTe specimen of varying thickness. For small specimen thicknesses (<250 nm) grain boundaries are not visible in the panchromatic CL image. Grain boundary contrast is produced by electron-hole recombination within the foil, and a large fraction of that light is lost to multiple-beam interference, so that thicker specimens are required before the grain boundary signal is above the TR background. This is undesirable for high spatial resolution. Furthermore, the CL spectrum contains additional features due to TR which are not part of the 'bulk' specimen. Strategies to minimise the effects of TR are also discussed.

P:37 Correlation between the atomic structure and spin-polarization at Co_2MnSi/Ag epitaxial interfaces

Z Nedelkoski[1], P Hasnip[1], A Sanchez[2], B Kuerbanjiang[1], E Higgins[1], M Oogane[3], A Hirohata[1], G Bell[2] and V Lazarov[1]

[1]University of York, UK, [2]University of Warwick, UK, [3] Tohoku University, Japan, UK

Understanding the correlation between the atomic structure and functionality in spin-electronic devices is crucial for their optimization as well as engineering novel type of devices. In this work we present joint experimental and theoretical study that directly correlates the atomic structure with the interface spin-polarization in half-metallic Heusler alloy based spin-valve device structures. Here, on the example of Co_2MnSi/Ag interface, a functional part of a spin-valve device, we study the effect of the electrode atomic plane(s) termination on the interface electronic properties. By employing density functional theory calculations we demonstrate clear difference in the spin polarization between the two bulk-like terminated interfaces: Co/Ag and Mn-Si/Ag. Strikingly, when the interface is determined by Co/Ag atomic planes the spin polarisation switches the sign (i.e. becomes negative) while the Mn-Si/Ag interface termination keeps the positive spin polarisation. Atomic structure analysis of fabricated spin-valve Co_2MnSi/Ag/Co_2MnSi heterostructures reveals the existence of a thermodynamically stable non-bulk atomic layer at the electrode/spacer interface. DFT calculations show that this layer introduces spin states of opposite spin polarisation compared to the rest of the electrode spin polarisation. This inversely spin polarised layer can act as an additional spin-scattering centre in this spin valve geometry. The strong dependence of the interface spin polarisation on the local atomic structure can be potentially used as a way to engineer the interface spin-polarization in spin device structures and hence tailor the overall device performance.

[1] Z Nedelkoski et al., The effect of atomic structure on interface spin-polarization of half-metallic spin valves: Co_2MnSi/Ag epitaxial interfaces, *Appl. Phys. Lett.* 107, 212404 (2015).

P:38 Oxides in austenitic alloys exposed to PWR primary water: mapping oxidation states with EELS

G Pimentel, J Dohr and S Lozano-Perez

University of Oxford, UK

Oxides in steels and Ni alloys exposed to Pressurized Water Reactor (PWR) primary water conditions are often layered structures of spinel oxides. As reported in previous works [1][2], these spinel oxides are rarely stoichiometric, resulting on a range of trivalent to divalent cations ratios. EELS has been traditionally used for qualitative and quantitative characterization of these oxides but can also provide information on coordination or valence [3]. Several studies can be found on how valence affects the location of the ionization edges L2 and L3 for transition metals or the ratio between white lines (L3/L2). In general, the trend tends to be that the edges move towards higher energy losses as the valence increases, with the metallic state (valence 0) having the lowest energy losses and the L3/L2 ratio decreases [4][5]. We have performed high energy resolution EELS analysis on various Fe, Cr and Ni oxides and considerable differences were observed (Figure 1) on the fine structure of Cr and Fe in different regions of, apparently, the same oxide phase. This suggests different oxidation states depending on the region which could explain the differences in densities observed and their relationship to fracture.

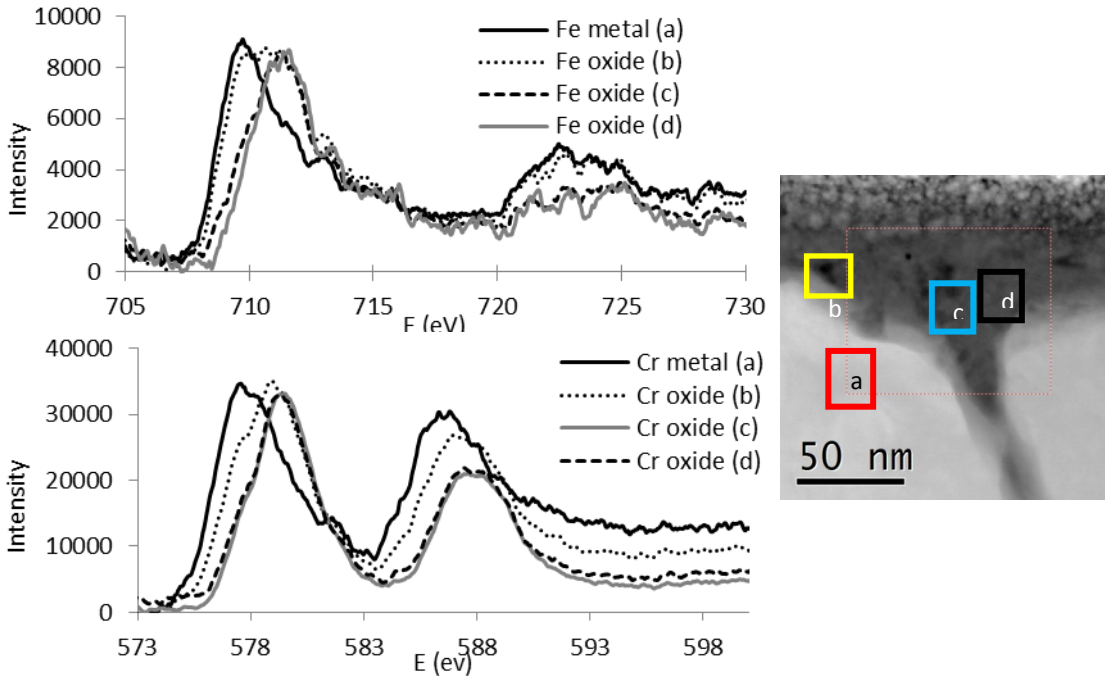

Figure 1: High energy resolution EELS spectra for Cr (top) and Fe (bottom) showing shifts in the L2 edge for the various regions boxed in the STEM HAADF image (right). Darker areas correspond to lower density oxide.

[1] Kruska, K, Chou, P, Calonne, O, Fournier, L, Lozano-Perez S, 16th International Conference on Environmental Degradation of Materials in Nuclear Power Systems-Water Reactors, Ashville, North Carolina, 2013

[2] Kruska, K, Lozano-Perez, S, Saxey, D W, Terachi, T, Yamada, T, Smith, G D W, Corrosion Science Vol.63, 2012, pp. 225-233

[3] Egerton, R, 2011, 3rd edition, Springer US

[4] Daulton, T L, Little, B.J., Ultramicroscopy, Vol.106, Iss.7, 2006, pp.561-573

[5] Tann, H, Verbeeck, J, Abakumov, A, Van Tendeloo, G, Ultramicroscopy, Vol.116, 2012, pp.24-33

P:39 Characterization of hydrogen stabilised polar MgO(111) thin films on 6H-SiC(0001)

D Pingstone[1], B Kurbanjan[1], L Lari[1], D Kepaptsoglou[2], Q Ramasse[2] and V K Lazarov[1]

[1]University of York, UK, [2]SuperSTEM, UK

In order to develop high power silicon carbide based MOSFETs that can surpass silicon based MOSFETs in performance, a stable oxide with sufficient dielectric constant is required to withstand the high voltage and high current that can be applied. Magnesium oxide, with rocksalt structure and high dielectric constant of 9.9 [1], has been proposed as a suitable gate oxide for SiC MOSFETs. However the polar structure of MgO(111) thin films, that has just 3% lattice mismatch with SiC(0001), introduces interesting physics from the diverging electrostatic potential associated with the polar (111) surface. The alternating anion and cation planes that stack along the (111) direction produce an electric polarization, leading to the diverging electrostatic potential with increasing layer thickness, that must be compensated by atomic and electronic reconstructions at the surface. These surfaces can reconstruct into <100> facets without stabilization [2]; a problem for producing multilayer heterostructures with MgO. One method for compensating the diverging potential leads to an offset of the valence band edge through charge transfer to the substrate [3]. This study uses monochromated XPS to determine the valence band offset of hydrogen stabilised MgO(111) thin films grown by plasma assisted molecular beam epitaxial growth on SiC(0001), characterised by scanning transmission electron microscopy (STEM) and electron energy loss spectroscopy (EELS) to understand the structural behaviour of polar MgO thin films for future device development. The valence band offset is also dependent on the interfacial atomic arrangement that can be determined using atomically resolved EELS to correlate the interface structure to valence band edge measurements for band offset engineering. The addition of hydrogen during the growth of the MgO thin films has reduced the roughness of the MgO surfaces by stabilising the polar <111> surface, as predicted [4].

[1] Subramanian M A., et al., Phys. Chem. Minerals, (1989) 16: 741-746
[2] Warot B, et al., Appl. Surf. Sci., (2002) 188: 151-155
[3] Zhang B, et al., Appl. Phys. Lett., (2008) 93: 072110
[4] Lazarov V K, et al., Phys. Rev. Lett., (2011) 107: 056101

P:40 HRTEM study of agglomeration of ZnO nanoparticles by oriented attachment

D G Rickerby[1], R Schneider[2], R Popescu[2], H Störmer[2] and D Gerthsen[2]

[1]European Commission Joint Research Centre, Italy, [2]Karlsruhe Institute of Technology (KIT), Germany

Oriented attachment is a widely recognised mechanism of crystal growth and agglomeration of crystalline nanoparticles. It occurs as a result of spontaneous realignment of neighbouring nanocrystals so that they share commonly oriented crystallographic planes and is an important process governing the self-assembly of nanoparticles into larger anisotropic crystal structures. As a general rule, attachment tends to take place principally on high surface energy planes, thereby acting to minimise the overall surface energy of the agglomerate itself. In the present work, investigations of agglomeration phenomena in dilute aqueous suspensions of zinc oxide nanoparticles were carried out using an aberration-corrected transmission electron microscope FEI Titan³ 80-300. The mean nanoparticle diameter determined by TEM was approximately 15 nm compared to a value of 240 nm measured by dynamic light scattering (DLS), indicating that there was significant agglomeration of the nanoparticles in suspension. Evidence for several different forms of oriented attachment was observed as shown in Fig. 1. These included the presence of contiguous crystallographic planes across crystal interfaces, low angle misoriented boundaries containing edge dislocations, and interfaces consisting of surface steps typically one or two atomic layers in height. Twin type relative orientations between adjacent nanocrystals were also seen in some cases. Interaction between an isolated pair of nanoparticles, in contact over a single interface, generally leads to coherent attachment, whereas when multiple nanocrystals are involved imperfect alignment may result due to rotation in

order to accommodate geometrically these additional crystallites into the structure. The results offer insights into factors controlling the manner in which nanocrystals agglomerate, and the influence that crystal defects and orientation have on this process.

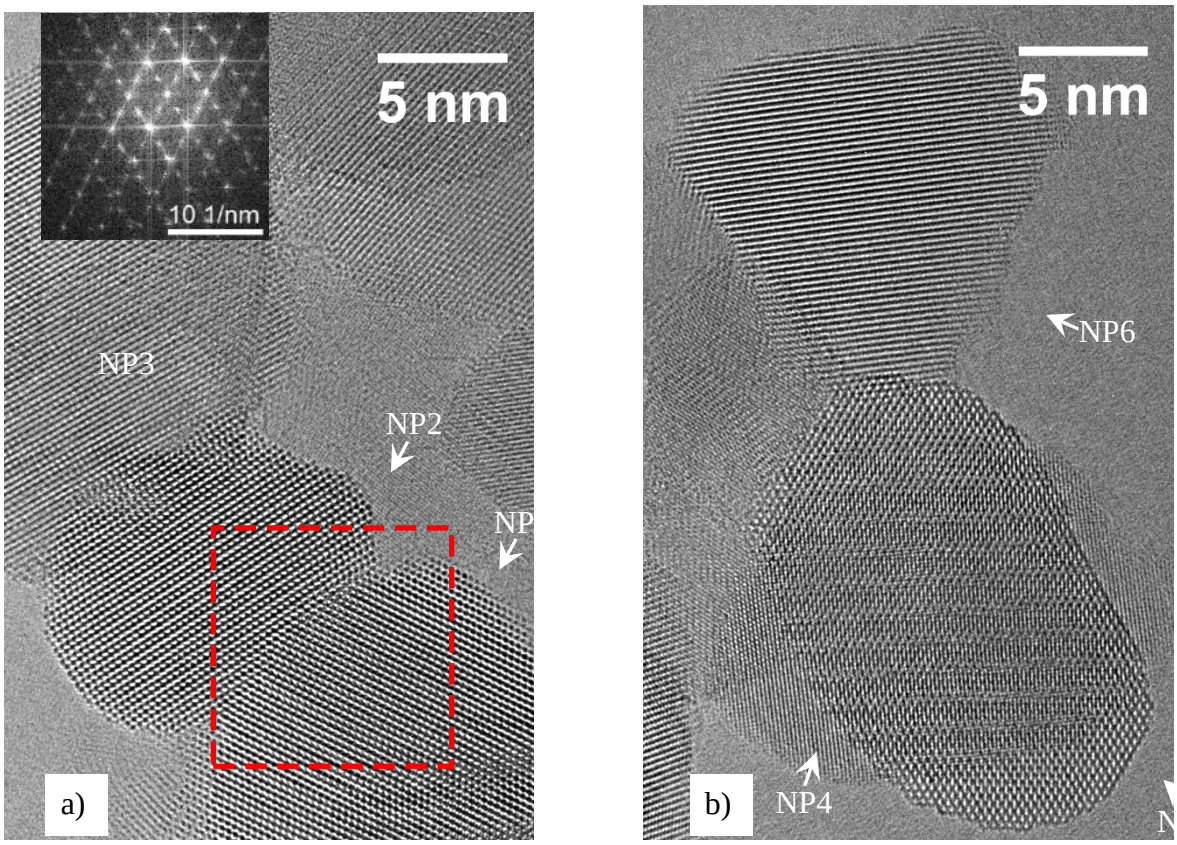

Fig. 1. High-resolution TEM images of ZnO nanoparticles showing contiguous crystallographic planes and grain boundaries between nanoparticles. For instance, in the case of Fig. 1a the two lower NPs 1 and 2 (cf. marked region) are arranged along the [110] direction parallel to the incident electron beam with an rotation angle of about 60° between them. The diffractogram (see inset) clearly shows this angular relationship. In contrast, only a small misorientation is observed between the lattice planes in NPs 2 and 3. In Fig. 1b the interface between NP5 and NP6 contains atomic level steps, while dissimilar types of lattice planes of differently orientated superimposed ZnO NPs, (e.g. NP4 and NP5), seem to be aligned to minimise surface energy.

P:41 3D structure mapping using a two-dimensional pixelated STEM detector

A Ross[1], M Nord[1], I Hallsteinsen[2], T Tybell[2] and I MacLaren[1]

[1]University of Glasgow, UK, [2]Norwegian University of Science and Technology, Norway

In perovskite oxide materials there is a strong coupling between structural and functional properties. Of recent interest are heterostructures, which enable structural coupling over the substrate/thin film interface. A common way of analysing the atomic structure of these heterostructures is using Scanning Transmission Electron Microscopy (STEM) which provide sub-Ångström resolution. Combining Annular Dark Field (ADF) and Annular Bright Field (ABF) imaging it is possible to get precise atom positions for all the atoms, even the light oxygen atom. However, these imaging techniques only reveal the structure orthogonal to the electron beam, yielding atomic structure information about two of the three axes. Normally, two separate TEM-samples thinned on orthogonal zone axis are used to get the 3-D structure. More ideal would be to obtain this information from one sample, such that information about all three axes in the same region can be gathered.

In this work, we have used a fast two-dimensional pixelated electron detector to acquire STEM-diffraction images of a $La_{0.7}Sr_{0.3}MnO_3/LaFeO_3$ heterostructure grown epitaxially on a $SrTiO_3$-(111) substrate. One diffraction image has been acquired for every probe position yielding a 4-D-datacube, covering the films and the substrate. By using Higher Order Laue Zones (HOLZ), information about crystal periodicity parallel to the electron beam is extracted. This data is processed using the model based approach, yielding information on both average and variations in lattice size as a function of distance from the interfaces. In co-junction with standard ABF and ADF characterisation a more complete understanding of the structure of these interfaces can be revealed.

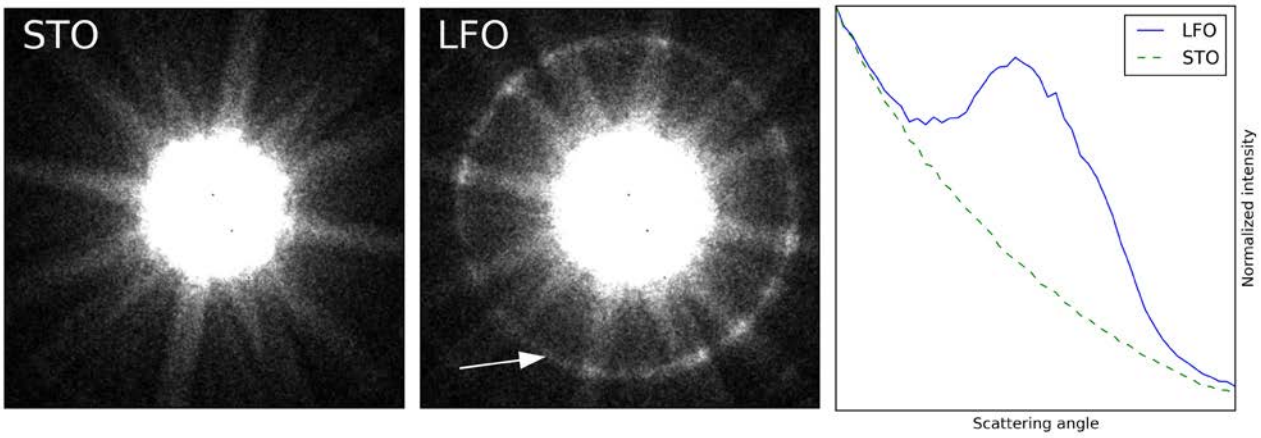

STEM diffraction images from $SrTiO_3$ (STO, left) and $LaFeO_3$ (LFO, middle). Arrow highlighting the HOLZ circle, which is due to the superstructure in LFO. Rightmost image: radial integration of the two diffraction images, showing the difference of intensity at the HOLZ scattering angles.

P:42 Aberration measurement in a probe-forming system using graphene

H Sawada[1,2] and A I Kirkland[1]

[1]University of Oxford, UK, [2]JEOL UK Ltd., UK

For operation of a STEM with aberration correctors, an accurate automated alignment system is required to adjust the residual aberrations. A typical system consists of automated aberration measurement and a suitable feedback module to the corrector. Accuracy in the aberration measurement for the probe-forming system is important to quantify the residual aberrations and the accuracy determines the final aberration free area for high-resolution observation after correction. Several methods to measure the aberration in STEM have been reported using nano-sized metal particles [1], and the analysis of ,beam induced image shifts on the Ronchigram [2], contrast transfer functions in the Ronchigram [3], a crystalline lattice [4,5], and a segmented Ronchigram from an amorphous film [6].

For more accurate measurement of aberrations in a corrected probe-forming system, a graphene lattice has will be reported in this study. The lattice parameter of graphene is known and changes in the lattice pattern with beam tilt or specimen tilt is smaller than that of the other crystalline specimens. In this work the Ronchigram was divided into local anglular areas to analyze local distortions by the probe-forming aberrations. The distortion in each local area was analyzed using an auto-correlation function. Six peaks surrounding the center peak of the auto-correlation function from a graphene image were identified and were fitted with an oval. Using the fitted parameters describing the oval shapes on local angular areas, the total aberration for the probe forming lens was calculated. Importantly, since the lattice parameter of a specimen is known, only one Ronchigram pattern is required to derive the aberration coefficients.

[1] M Haider, S Uhlemann, and J Zach Ultramicroscopy 81 (2000) 163
[2] N Dellby, O L Krivanek, P D Nellist, P E Batson, A R Lupini, J. Electron Microsc. 50 (2001) 177
[3] A R Lupini, P Wang, P D Nellist, A I Kirkland, and S J, Pennycook Ultramicroscopy 110 (2010) 891
[4] A R Lupini, and S J Pennycook, J Electron Microsc.57 (2008) 195
[5] T Yamazaki, et al, Ultramicroscopy 106 (2006) 153
[6] H Sawada, et al, Ultramicroscopy 108 (2008) 1467

P:43 Off-axial aberration measurement for the image-forming system of a hexapole type aberration corrector

H Sawada[1,2,], S Morishita[3], T Nakamichi[3], F Hosokawa[4], K Suenaga[5] and A I Kirkland[1]

[1]University of Oxford, UK, [2] JEOL UK Ltd., UK, [3]JEOL Ltd, Japan, [4]BioNet Ltd, Japan, [5]National Institute of Advanced Industrial Science and Technology (AIST), Japan

High resolution observation of extended areas of mono-layered materials, for example graphene, using large field of view cameras, using transmission electron microscopy are key to understanding defects and their evolution. Structural study for this radiation sensitive material requires observation at a low accelerating voltage in the TEM to reduce damage. However, when operating a TEM at low accelerating voltage, off-axial aberrations often increase due to the shorter focal length of the objective lens. These off-axial aberration affect the aberration free condition at the surrounding areas of the field of view, resulting in difficulties in the interpretation of all atomic positions from experimental images. It is therefore, important to measure off-axial aberrations and to achieve optimum aberration conditions for analyzing experimental images with wide fields of view.

In this study, we will report measurement of off-axial aberrations using diffractogram tableaus from different positions in the experimental image field of view [1]. When excitation of the transfer lenses between the objective lens and the corrector were changed, the off-axial defocus increases. In the case where the excitation of the transfer lenses between the hexapoles was changed, the measured off-axial aberration showed an off-axial two-fold astigmatism, with a three-fold symmetry across the field of view. A part of this work was supported by the JST under the Research Acceleration Program.

[1] I Maßmann, S Uhlemann, H Müller, P Hartel, J Zach., M Haider, Y Taniguchi, D Hoyle, and R Herring, Microsc. Microanal. 17 Suppl. (2011) 1270

P:44 Planar FIB milling of copper by using the novel rocking stage technology

S Sharang[1], A Benkouider[1], T Hrncir[2], J V Obona[2], J Jiruse[2] and E Principe[3]

[1]Tescan Orsay Holding, Czech Republic, [2]Tescan Brno, Czech Republic, [3]Tescan USA, USA

Copper has found immense applications within the semiconductor industry. In order to make site-specific alterations using focused ion beam (FIB) at nanoscale levels, it is imperative we manage to operate on polycrystalline copper directly with no need for an extensive grain size and orientation study prior to performing FIB milling operations. Homogenous copper FIB milling arises from the need to perform various circuit edit operations below the dielectric layer following the copper layer. If the layer beneath the dielectric is affected by inhomogeneous milling, it can lead to short-circuit and eventual device breakdown [1-2]. Failure analysis on an integrated circuit was performed using rocking stage with 6-axes piezo movement capabilities together with the novel approach of the combined Xe-plasma ion source FIB and SEM system (XEIA) [3-5]. Site-specific milling of copper with different milling strategies were tested to optimize time and homogeneity of the milling across the target surface and to overcome the channelling effect posed by polycrystalline copper. Only during the last few nanometres of copper layer the water vapour is used to protect the dielectric layer. The complete removal of copper was followed with XeF_2 assisted milling of the dielectric layer to observe the unharmed circuitry [6]. Channelling effect was reduced by regulating the sputtering rates across different grains keeping the underlying dielectric layer safe. High-resolution scanning electron microscopy (HR-SEM) imaging was used for constant monitoring of the removed material to help modulate the process for highest throughput in the least possible amount of time.

[1] Tahir Malik et.al, *36th ISTFA Proceedings* (2010)
[2] EAG White paper – FIB Circuit Edit, Feb 2014
[3] T Hrnčíř et al, *38th ISTFA Proceedings* (2012)
[4] Jaroslav jiruse et.al, *Microsc. and Microanal.* 18 (2012)
[5] T Hrnčíř et al, *Microsc. and Microanal.* 19 (2013)
[6] Chad Rue et.al. *33rd ISTFA Proceedings* (2007)

P:45 Wear behaviour of high-performance C-Mo-W coatings investigated by multi-technique aberration corrected TEM

J Sharp[1], I Castillo Muller[1], P Zeng[1], P Mandal[2], M Rainforth[1], P Hovsepian[2] and A Ehiasarian[2]

[1]University of Sheffield, UK, [2]Sheffield Hallam University, UK

We have previously presented a high-performance wear resistant coating made by duplex sputtering: C is deposited by unbalanced magnetron sputtering, with Mo and W added by the High Impact Plasma Induced Magnetron Sputtering (HIPIMS) process from a compound target. These coatings can survive higher temperatures than DLC coatings, making them of interest for applications such as auto engines. The structure consists of 2-5 nm onion-like clusters of carbon, in which the Mo and W are mostly localised. These are arranged into disordered sheets (stripes in a TEM cross section); the degree of cluster segregation into sheets varies periodically with depth, producing a second, wider set of meta-stripes.

Samples of the coating deposited on steel were wear-tested using stainless steel and alumina ball counterfaces at room temperature. We will concentrate here on those with load of 4N and 1km total distance. FIB cross-section samples were made from the middle of the wear track and characterised on the JEOL R005 double aberration FEGTEM at Sheffield University (300 kV). TEM, STEM, EELS and EDS were used. The films showed lower friction with the alumina counterface but less material lost during the test with the steel counterface.

The alumina counterface produced a carbon tribolayer 3-3.5 nm thick on an extremely flat wear surface. The first layer of clusters under the wear surface showed some that appear to have “unrolled”; under this first layer the structure was unchanged from the as-deposited coating. In the tribolayer were found high-Z particles of 1-2 nm in size; EDS found these to contain W, as if released from the unrolled clusters.

The steel counterface produced a tribolayer ~30 nm thick, made of coarse pieces of material. EDS and EELS showed this material contained C, Mo, W, Fe and Cr; this is a reaction product between the steel counterface and the film, and the beginning of the wear test indicated stick-slip occurring. The material in the wear track has aggregated into pieces of ~10 nm size. This material adhering to the surface is the cause of the lower wear rate in the steel test despite the higher coefficient of friction.

P:46 Quantitative grain boundary analysis with atom probe tomography and t-EBSD (TKD)

Y Chen[1], K P Rice[1], T J Prosa[1], R M Ulfig[1] and I Holton[2]

[1]CAMECA Instruments, Inc., USA, [2]Acutance Scientific Ltd., UK

Thermal barrier coatings (TBCs) allow turbine engines to be operated at temperatures greater than the melting temperatures of engine components to pursue better propulsive power performance and fuel efficiency [1]. TBCs generally consist of three layers. On the top is a coat made of yttrium-stabilized ZrO_2 (or YSZ) which has excellent thermal resistivity. Beneath the YSZ layer is a thermally grown oxide (TGO) scale that consists of -alumina grains. At the coating/substrate interface is a bond coat layer that improves adhesion of the ceramic layers on the superalloy substrate. Atom probe tomography (APT) was previously used to quantify grain boundary chemistry in TGO layers. Significant chemical variations between different grain boundaries were reported, suggesting a strong effect of grain boundary character [2].

Inspired by the ability of mapping needle shaped specimens using electron backscatter diffraction (EBSD) in transmission mode, this work aims to further investigate the relationships between grain boundary chemistry and grain boundary misorientation using the integrated APT/t-EBSD technique [3]. The integrated EXAX EBSD system allows for in-situ mapping feedback between milling processes. Grain boundaries were successfully captured by APT and their structures and chemistries were studied accordingly.

In this study we have demonstrated that high-resolution t-EBSD maps can be acquired on needle-shaped APT specimens that consist of alumina grains of size ranging from few hundred nanometers to few micrometers. Transmission EBSD mapping offers the ability to target site-specific grains for APT analysis, and correlate grain boundary chemistries with grain misorientations. In addition, we succeeded in collecting multiple APT datasets and t-EBSD maps from a single APT specimen, thus the evolution of structure across TGO scales can be investigated.

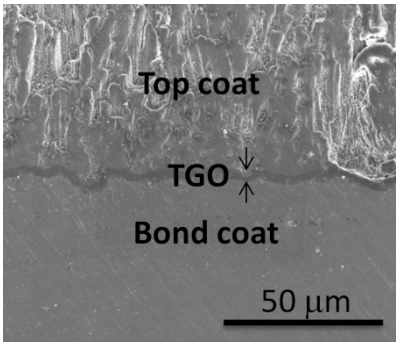

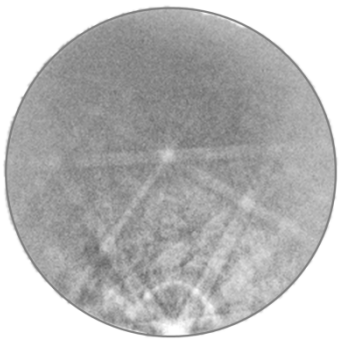

Figure 1. SEM image of TBC with a 3 *-based superalloy.*
Figure 2. A typical EBSD pattern of -alumina collected with 30 kV electrons

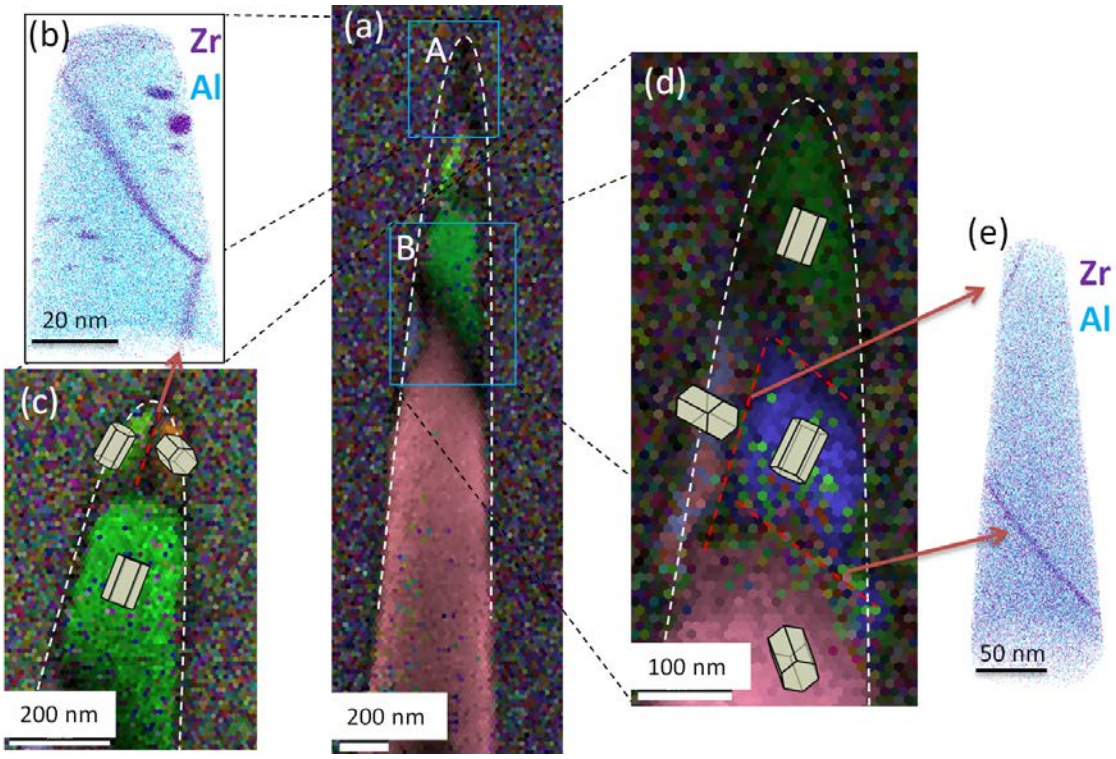

Figure 3. t-EBSD maps of alumina grains and correlative APT results from region A and

[1] A Evans *et al.*, Prog Mater Sci 46 (2001), p. 505
[2] Y Chen *et al.*, Oxidation of Metals 82 (2014), p. 457
[3] K Babinsky *et al.*, Ultramicroscopy 144 (2014), p. 9

P:47 Detailed atomic reconstruction of extended line defects in monolayer MoS_2

S Wang[1], G-D Lee[2], K He[1] and J H Warner[1]

[1]University of Oxford, UK, [2]Seoul National University, Korea

Monolayer molybdenum disulphide (MoS_2) has become complementary to gapless graphene due to its direct band gap, which shows great potential for applications in nanoelectronics, optoelectronics and flexible devices.[1] Electron beam irradiation of monolayer MoS_2 at accelerating voltages of 80kV preferentially generates S vacancies that aggregate into extended line defects with subtle lattice reconstructions.[2] Accurate measurements of the atomic positions within line defects is required for precise theoretical models to predict their electronic and magnetic properties. I will present results that show how monochromation of electron source in an aberration-corrected transmission electron microscope (AC-TEM) helps reduce chromatic aberration effects and produce high spatial resolution images that reveal the fine structure of S atomic positions at line defects, figure 1. Atomic models deduced from AC-TEM are verified by density functional theory (DFT) calculations, showing measureable bond reconstructions arising from missing S atoms. Bond length variations as function of the line defect's length and width are observed, with lattice compression along the armchair direction as the line defects extend. Atomistic scale strain fields and lattice distortion at line defects are quantified by mapping the exact location of each atom in the defective region. The evolution dynamics of line defects under the electron beam irradiation are also investigated, including extension, stack, translation and deflection. DFT calculations predict the evolution of electronic properties

for line defects with an expanded width, gradually transforming from semiconducting to metallic. These results provide important insights into how defect structures could be used for creating metallic tracks within semiconducting monolayer MoS_2 films for future applications in electronics and optoelectronics. Figure 1. An aberration corrected TEM image of CVD-grown monolayer MoS_2, showing a S line defect produced by electron beam irradiation.

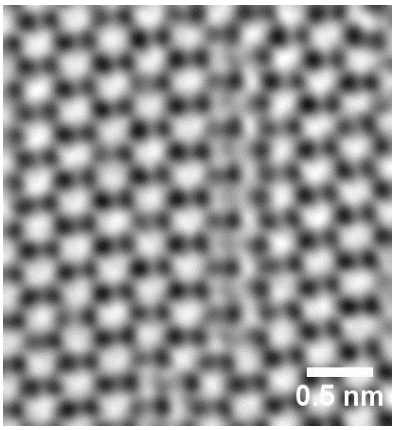

Figure 1. An aberration corrected TEM image of CVD-grown monolayer MoS_2, showing a S line defect produced by electron beam irradiation.

[1] Mak, K F; Lee, C; Hone, J; Shan, J and Heinz, T F Atomically Thin MoS_2 : A New Direct-Gap Semiconductor Phys. Rev. Lett. 2010, 105, 136805.

[2] Komsa, H-P; Kurasch, S; Lehtinen, O; Kaiser, U and Krasheninnikov, A V From Point to Extended Defects in Two-Dimensional MoS2: Evolution of Atomic Structure Under Electron Irradiation. Phys. Rev. B 2013, 88, 035301.

P:48 Investigation of phase separation in InGaN semiconductor alloys by plasmon loss spectroscopy

X Wang[1], P Ruterana[2] and T Walther[1]

[1]University of Sheffield, UK, [2]CIMAP UMR 6252, France

Phase separation in InGaN alloys, as predicted by Ho and Stringfellow [1] and later observed by several groups [2-6], can strongly affect the optical properties, especially for high indium concentrations [7]. Therefore it is important to quantify the degree of phase separation. InGaN samples grown with high III/V flux ratios at high temperatures are particularly prone to phase separation. Previously, the degree of phase separation could only be reliably quantified by Rutherford backscattering, as transmission electron microscopy (TEM) could lead to beam damage due to the radiation sensitivity of InGaN [8,9]. High electron fluxes as typically used in high-resolution TEM or core-loss electron energy-loss spectroscopy (EELS) may lead to erroneous results. On the contrary, low-loss EELS can yield useful spectra of the plasmon loss regions at much lower electron fluxes thus potentially reducing beam damage in the TEM. Unfortunately, the low energetic core losses of Ga M and In N edges partially overlap with the plasmon peaks.

Here we demonstrate a new method to quantify phase separation in InGaN by fitting both plasmon and core losses over the region of 13-30eV. First, we fit Lorentz functions to the main plasmon peaks. In previous work [10], we directly correlated the chemical shift of the plasmon peak position with the indium concentration, which works in the absence of phase separation. From the measured chemical shifts of the core-losses, we have constructed reference spectra for each indium concentration. Finally, we apply multiple linear least-squares (MLLS) regression to fit each experimental spectrum as a weighted superposition of reference spectra of pure GaN, pure InN and an $In_xGa_{1-x}N$

alloy. For x=0.3 and x=0.59, the relative contributions of the binary compounds are negligibly small and indicate random alloys. For $x_{nominal}$=0.62, we found strong indication for phase separation, manifested by the need to include significant contributions of GaN and InN to explain the broadened plasmon peaks in some of the spectra where energy-dispersive X-ray spectroscopy suggested an average indium content of <x>=0.68.

[1] I Ho and G. B. Stringfellow , *Appl. Phys. Lett.* 69, 2701 (1996)
[2] N A El-Masry et al., *Appl. Phys. Lett.* 72, 40–42 (1998)
[3] S Yu Karpov,MRS Internet J. Nitride Semicond. Res., 3, pp e16 (1998)
[4] M Rao,D Kim and S. Mahajan, *Appl. Phys. Lett.* 85, 1961-1963 (2004)
[5] A Koukitu et al., *J. Cryst. Growth.*197, 99-105 (1999)
[6] P Ruterana, G Nouet, W Van der Stright, I Moerman and L Considine, *Appl. Phys. Lett.* 72, 1742 (1998)
[7] R Singh et al., *Appl. Phys. Lett.*70,1089 (1997)
[8] J P O'Neill et al., *Appl. Phys. Lett.* 83, 1965-1967 (2003)
[9] T M Smeeton et al., *Appl. Phys. Lett.* 83, 5419-5421 (2003)
[10] X Wang et al., *Semicond. Science Technol.*30, 114011(2015)

Institute of Physics
76 Portland Place, London W1B 1NT, UK
Telephone: +44 (0)20 7470 4800
www.iop.org/conferences

Registered Charity Number: 293851